

The RNA-binding protein PTBP1 is necessary for B cell selection in germinal centers

Elisa Monzón-Casanova^{1,2}, Michael Screen¹, Manuel D. Díaz-Muñoz¹, Richard M. R. Coulson¹, Sarah E. Bell¹, Greta Lamers¹, Michele Solimena^{3,4,5,6}, Christopher W. J. Smith^{1,2} and Martin Turner^{1*}

Antibody affinity maturation occurs in germinal centers (GCs), where B cells cycle between the light zone (LZ) and the dark zone. In the LZ, GC B cells bearing immunoglobulins with the highest affinity for antigen receive positive selection signals from helper T cells, which promotes their rapid proliferation. Here we found that the RNA-binding protein PTBP1 was needed for the progression of GC B cells through late S phase of the cell cycle and for affinity maturation. PTBP1 was required for proper expression of the c-MYC-dependent gene program induced in GC B cells receiving T cell help and directly regulated the alternative splicing and abundance of transcripts that are increased during positive selection to promote proliferation.

Germinal centers (GCs) are specialized areas of secondary lymphoid tissues in which B cells undergo antibody affinity maturation. The GC can be divided into a dark zone (DZ), characterized by extensive proliferation and somatic hypermutation, and a light zone (LZ), where B cells are less proliferative and make contacts with follicular dendritic cells and T cells. There, B cells are positively selected to survive and undergo further rounds of proliferation in the DZ^{1,2}. Help provided by T cells promotes faster progression through the cell cycle, a greater number of cell divisions and increased frequency of somatic hypermutation, which results in increased antibody affinity maturation^{3,4}. Positive selection in the LZ results in the transient expression of the transcription factor c-MYC necessary for the progression of selected cells through the cell cycle^{5,6}. c-MYC also induces the transcription of genes encoding products important for anabolic metabolism^{3,7}. Moreover, activity of the metabolic checkpoint kinase complex mTORC1 is increased during positive selection and promotes the anabolic gene-expression program⁸. In addition to c-MYC, the transcription factors AP4, FOXO1 and BATF are important during the LZ–DZ transition of GC B cells^{9–11}. Such findings highlight the existence in B cells of relays of transcription factors that are responsive to T cell help and promote B cell proliferation and mutation.

Alternative splicing (AS), alternative polyadenylation (APA), mRNA decay and translation have the potential to regulate cell fate. However, relatively little is known about the relevant changes in and regulation of AS during immune responses^{12–15}, and the molecular regulation of APA is only beginning to be appreciated^{16,17}. The impact of RNA-binding proteins (RBPs) that have the potential to integrate multiple aspects of gene expression in B cells undergoing selection in the GC is only emerging^{13,14}.

One class of RBPs with pleiotropic functions is the polypyrimidine tract-binding proteins (PTBPs)^{18–20}. Most cell types express PTBP1, whereas PTBP2 is abundant in differentiated neurons. During neuronal differentiation, there is a switch between the expression of PTBP1 and that of PTBP2, which drives changes in the AS patterns of genes encoding products important for neuronal

function^{18,21}. PTBP3 has high expression in hematopoietic cells and has been shown to be co-expressed with PTBP1 in B lymphocytes²². PTBP1 is both a repressor of AS and an activator of AS¹⁸ and has been linked to APA, mRNA decay and translational regulation^{19,23,24}. In CD4⁺ T cells, PTBP1 has been shown to enhance the stability of mRNA encoding the B cell-stimulatory molecule CD40L²⁵, and in human B cells, it has been shown to be responsive to the receptor TLR9²⁶. Although PTBP1 has the potential to regulate post-transcriptional gene-expression programs in lymphocytes, its physiological functions in the development and activation of lymphocytes are unknown.

Here we found that PTBP1 acted in concert with c-MYC to ensure the selection of B cell clones with the highest affinity for antigen by promoting the proliferation of GC B cells. PTBP1 guaranteed proper post-transcriptional processing and the expression of genes induced as part of the c-MYC-dependent gene-expression program.

Results

PTBP1 expression is increased in positively selected GC B cells.

In contrast to the expression of mRNA encoding other members of the PTBP family, the expression of *Ptbp1* mRNA was ~1.5-fold higher in GC B cells than in naive B cells (Supplementary Fig. 1a,b). *Ptbp2* transcripts were rare and showed evidence of skipping of exon 10 (Supplementary Fig. 1b), which generates mRNAs degraded by nonsense-mediated RNA decay (NMD)²⁷. *Ptbp1* mRNA increased 1.4-fold after c-MYC expression in LZ B cells, but *Ptbp3* mRNA did not (Fig. 1a), and *Ptbp1* mRNA was also increased in GC B cells that had received the greatest levels of T cell help, relative to its abundance in GC B cells that had received less help from T cells (Supplementary Fig. 1c,d). A panel of monoclonal antibodies validated as recognizing PTBP1, PTBP2 or PTBP3 that were specific for each PTBP and able to detect the proteins by flow cytometry (Supplementary Fig. 2a,b) detected PTBP1 and PTBP3, but not PTBP2, in B cells (Fig. 1b and Supplementary Figs. 1f and 2a,b). PTBP1 protein was ~1.6-fold more abundant in GC B cells than in non-GC B cells (Fig. 1b) and was ~1.4-fold more abundant in GC

¹Laboratory of Lymphocyte Signaling and Development, The Babraham Institute, Cambridge, UK. ²Department of Biochemistry, University of Cambridge, Cambridge, UK. ³Molecular Diabetology, University Hospital and Faculty of Medicine, Technische Universität Dresden, Dresden, Germany.

⁴Paul Langerhans Institute Dresden of the Helmholtz Center Munich at University Hospital and Faculty of Medicine, Technische Universität Dresden, Dresden, Germany. ⁵Max Planck Institute for Molecular Cell Biology and Genetics, Dresden, Germany. ⁶German Center for Diabetes Research (DZD e.V.), Neuherberg, Germany. *e-mail: martin.turner@babraham.ac.uk

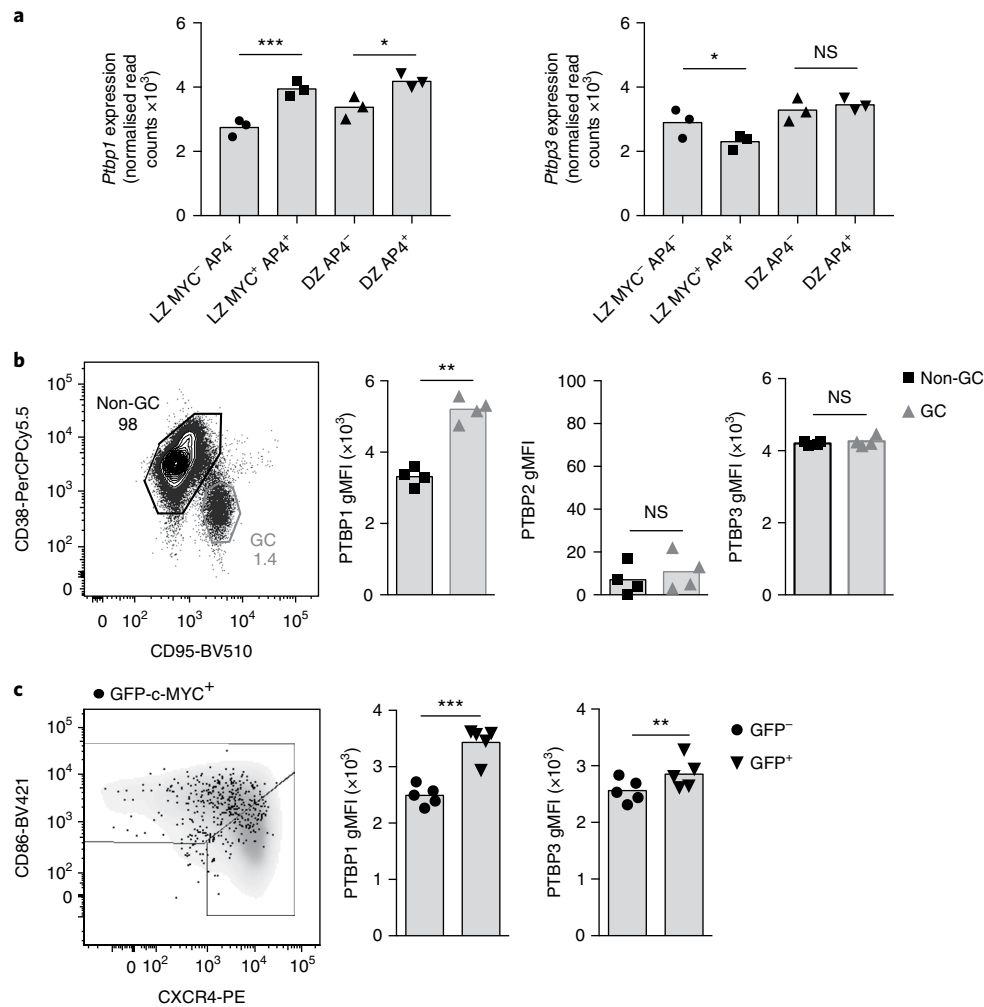


Fig. 1 | PTBP1 expression is increased in positively selected GC B cells. a, mRNAseq analysis of *Ptbp1* and *Ptbp3* in GC B cell populations sorted by expression of c-MYC and AP4⁷ (horizontal axis), presented as normalized read counts (from DESeq2 software for the analysis of differential gene expression on the basis of negative binomial distribution). NS, not significant ($P > 0.1$); * $P < 0.05$ and *** $P < 0.001$ (DESeq2; adjusted P values). **b**, Gating strategy for GC and non-GC B cells (left) (full gating strategy, Supplementary Fig. 1e), and expression of PTBP1, PTBP2 and PTBP3 (middle and right) by the gated populations (key), analyzed by flow cytometry 7 d after immunization of mice with NP-KLH and presented as geometric mean fluorescence intensity (gMFI) for each antibody after subtraction of background staining with isotype-matched control antibodies (Supplementary Fig. 1f). Numbers adjacent to outlined areas (left) indicate percent cells in each gate. **c**, Flow-cytometry analysis of the expression of the costimulatory molecule CD86 and the chemokine receptor CXCR4 (left) by GFP-c-MYC⁺ GC B cells (dots) and GFP-c-MYC⁻ GC B cells (shading), and of the expression of PTBP1 and PTBP3 (middle and right) in GFP-c-MYC⁺ and GFP-c-MYC⁻ GC B cells (key) from *Myc*^{GFP/GFP} mice 6 d after immunization with SRBCs. Each symbol represents an individual mRNAseq library (**a**) or mouse (**b,c**); bar tops indicate the mean. NS, not significant ($P > 0.1$); ** $P < 0.01$ and *** $P < 0.001$ (two-tailed paired Student's t -test (**b,c**)). Data are representative of three independent experiments (**b**) or one experiment (**c**).

B cells positive for a reporter transgene (*Myc*^{GFP}) encoding green fluorescent protein (GFP)-tagged c-MYC (GFP-c-MYC) than in GC B cells negative for GFP-c-MYC (Fig. 1c). Published studies have shown that PTBP1 expression correlates positively with c-MYC²⁸ and that c-MYC binds to the promoter of the gene encoding PTBP1 in B cells²⁹. Thus, PTBP1 might act downstream of, or in parallel with, c-MYC in GC B cells responding to help from T cells.

PTBP1 is dispensable for B cell development. We next studied mice with conditional knockout (cKO) of *loxP*-flanked *Ptbp1* alleles (*Ptbp1*^{fl/fl})³⁰, from the pro-B cell stage onward, via Cre recombinase expressed from the locus encoding the immunoglobulin α -chain CD79A (*Cd79a*^{Cre}) and confirmed the absence of PTBP1 protein at the appropriate stage (Supplementary Fig. 2b–d). B cell development was normal in the absence of PTBP1 (Supplementary Fig. 2c,e,f). Moreover, in lethally irradiated CD45.1⁺ B6.SJL mice reconstituted

with a 1:1 mixture of bone marrow cells from B6.SJL mice and *Cd79a*^{Cre/+}*Ptbp1*^{fl/fl} mice, the number of follicular B cells that arose from the *Cd79a*^{Cre/+}*Ptbp1*^{fl/fl} (cKO) bone marrow was not lower than the number of such cells that arose from B6.SJL bone marrow (data not shown). In cells that had deleted *Ptbp1*, expression of PTBP2 was evident from the pro-B cell stage onward (Supplementary Fig. 2d). The loss of PTBP1 and expression of PTBP2 was confirmed by immunoblot analysis (Supplementary Fig. 2a). As expected³¹, *Ptbp1*-deficient B cells also contained a greater amount of the long isoform of PTBP3 than did *Ptbp1*-sufficient B cells (Supplementary Fig. 2a). This indicated that although PTBP1 was not necessary for B cell development, its deletion was consequential at the molecular level.

PTBP1 in B cells is necessary for the GC B cell response. We immunized *Cd79a*^{Cre/+}*Ptbp1*^{fl/fl} and *Cd79a*^{+/+}*Ptbp1*^{fl/fl} mice with 4-hydroxy-3-nitrophenyl-acetyl conjugated to keyhole limpet

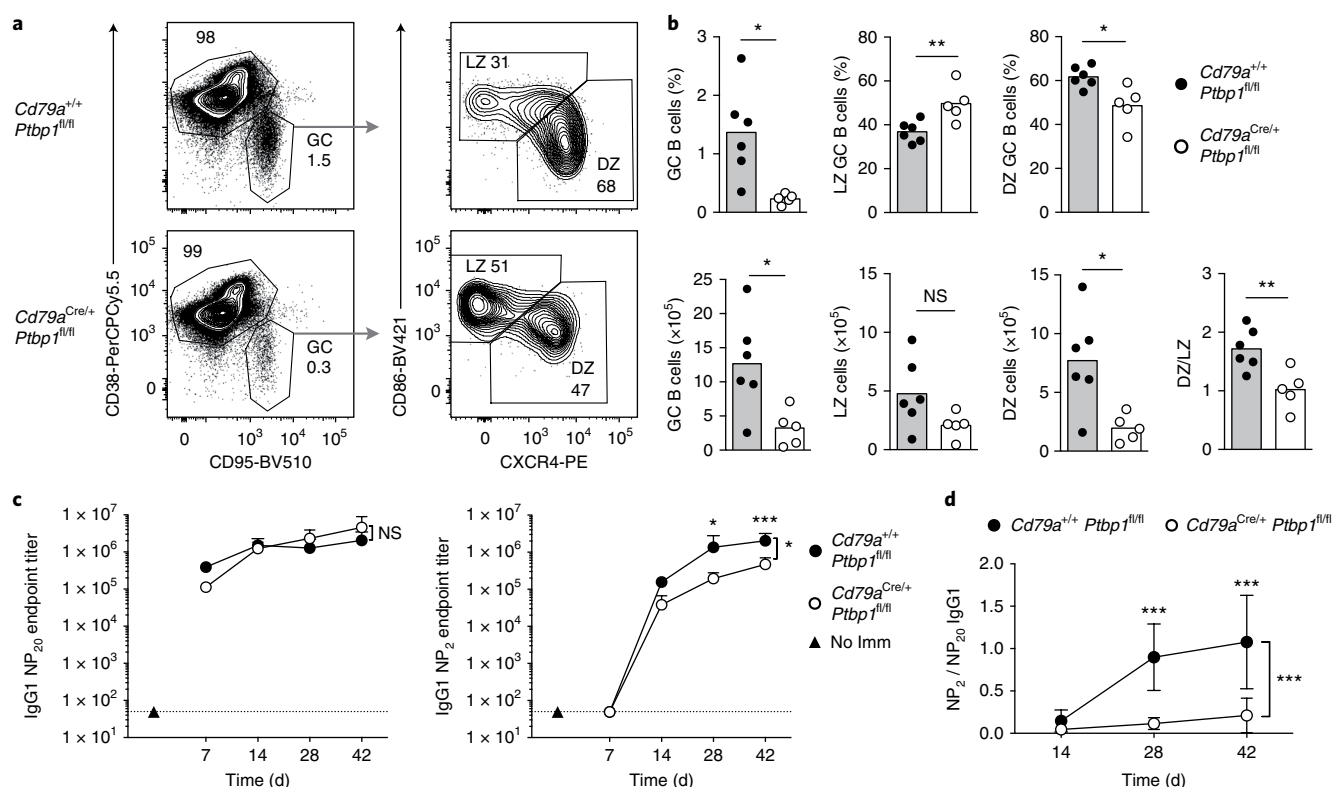


Fig. 2 | PTBP1 is necessary for GC B cell responses. **a**, Gating strategy for GC B cells (left) and LZ and DZ GC B cells (right) from the spleen of *Cd79a^{+/+}Ptbp1^{fl/fl}* and *Cd79a^{Cre/+}Ptbp1^{fl/fl}* mice (left margin) 7 d after immunization with NP-KLH, pre-gated on B220⁺CD19⁺ cells at left. Numbers in outlined areas indicate percent cells in each gate. **b**, Frequency (top row) and number (bottom row) of GC B cells and DZ and LZ GC B cells in mice as in **a** (key), identified as in **a**, and ratio of DZ GC B cells to LZ GC B cells (DZ/LZ) in such mice (bottom right). Each symbol represents an individual mouse in one experiment; bar tops indicate the mean. NS, not significant ($P > 0.05$); * $P < 0.05$ and ** $P < 0.01$ (two-tailed unpaired Student's *t*-test). **c**, ELISA of the endpoint titers of anti-NP₂₀ IgG1 (high- and low-affinity IgG1; left) or anti-NP₂ IgG1 (high-affinity IgG1 only; right) in the serum of *Cd79a^{+/+}Ptbp1^{fl/fl}* and *Cd79a^{Cre/+}Ptbp1^{fl/fl}* mice (key) at various times (horizontal axis) after immunization with NP-KLH. **d**, Ratio of anti-NP₂ IgG1 to anti-NP₂₀ IgG1 (NP₂ / NP₂₀), calculated from the data in **c**. NS, not significant ($P > 0.05$); * $P \leq 0.05$ and *** $P \leq 0.0002$, *Cd79a^{+/+}Ptbp1^{fl/fl}* versus *Cd79a^{Cre/+}Ptbp1^{fl/fl}* (two-way analysis of variance (ANOVA) plus Sidak's multiple-comparisons test). Data are from one experiment representative of four independent experiments (**a,b**) or one experiment representative of two independent experiments with similar results, with three *Cd79a^{+/+}Ptbp1^{fl/fl}* mice and six *Cd79a^{Cre/+}Ptbp1^{fl/fl}* mice (**c,d**; mean + s.d. (**c**) or mean ± s.d. (**d**)).

hemocyanin (NP-KLH). 7 d later, the proportion and absolute number of GC B cells per spleen were lower (5.9-fold and 3.9-fold, respectively) in *Cd79a^{Cre/+}Ptbp1^{fl/fl}* (cKO) mice than in *Cd79a^{+/+}Ptbp1^{fl/fl}* (control) mice (Fig. 2a,b). The proportion of GC B cells with a DZ phenotype was lower in *Ptbp1*-deficient GC B cells than in *Ptbp1*-sufficient (control) GC B cells (Fig. 2a,b), despite efficient depletion of the protein in the cells (Supplementary Fig. 3a). In contrast, *Cd79a^{Cre/+}Ptbp1^{fl/fl}* mice immunized with NP-KLH showed GC B cell responses similar to those of *Cd79a^{+/+}Ptbp1^{fl/fl}* mice (Supplementary Fig. 3b,c). The same GC B cell defects were found in *Cd79a^{Cre/+}Ptbp1^{fl/fl}* (cKO) GC B cells from B6.SJL chimeras reconstituted with a 1:1 mixture of bone marrow cells from CD45.1⁺ B6.SJL mice and CD45.2⁺ *Cd79a^{Cre/+}Ptbp1^{fl/fl}* (cKO) mice (Supplementary Fig. 3d,e). Therefore, the defect in *Ptbp1*-deficient GC B cells was cell autonomous. These data indicated an indispensable role for the function of PTBP1 in GC B cells.

PTBP1 is necessary for antibody affinity maturation.

Cd79a^{Cre/+}Ptbp1^{fl/fl} (cKO) mice produced lower amounts of high-affinity antibodies than did *Cd79a^{+/+}Ptbp1^{fl/fl}* (control) mice (Fig. 2c). In *Cd79a^{+/+}Ptbp1^{fl/fl}* (control) mice, the ratio of high-affinity antibodies to high- and low-affinity antibodies increased over time, but this ratio remained low in *Cd79a^{Cre/+}Ptbp1^{fl/fl}* (cKO) mice (Fig. 2d). Antibodies from mice lacking *Ptbp2* in B cells (*Cd79a^{Cre/+}Ptbp2^{fl/fl}*)

mice) showed no defect in affinity maturation relative to that of antibodies from *Cd79a^{+/+}Ptbp2^{fl/fl}* mice (Supplementary Fig. 3f,g). *Cd79a^{Cre/+}Ptbp1^{fl/fl}* (cKO) GC B cells had switched to immunoglobulin G1 (IgG1) in vivo at a greater frequency than had *Cd79a^{+/+}Ptbp1^{fl/fl}* (control) GC B cells (Supplementary Fig. 3h), which indicated the presence of functional activation-induced cytidine deaminase (AID) in *Ptbp1*-deficient GC B cells. Additionally, mutations were found at a similar frequency in the intronic region of the gene encoding heavy-chain joining region 4 in GC B cells sorted from *Cd79a^{Cre/+}Ptbp1^{fl/fl}* mice and those from *Cd79a^{+/+}Ptbp1^{fl/fl}* mice (Supplementary Fig. 3i,j). Thus, PTBP1 was necessary in B cells for optimal antibody affinity maturation, but this probably did not stem from diminished function of AID.

PTBP2 partially compensates for the loss of PTBP1 in GC B cells.

The expression of PTBP2 in *Ptbp1*-deficient GC B cells might compensate for the absence of PTBP1 in GC cells^{31,32}. To address this in the absence of confounding effects due to the deletion of genes during the bone marrow stages of B cell development, we introduced a transgene encoding Cre expressed under the promoter of the gene encoding AID (*Aicda*Tg-Cre) to generate mice with single conditional knockout of *Ptbp1* alone (*Aicda*Tg-Cre*Ptbp1^{fl/fl}* (cKO)) or double conditional knockout of both *Ptbp1* and *Ptbp2* (*Aicda*Tg-Cre*Ptbp1^{fl/fl}Ptbp2^{fl/fl}* (dcKO)). After immunization with sheep red

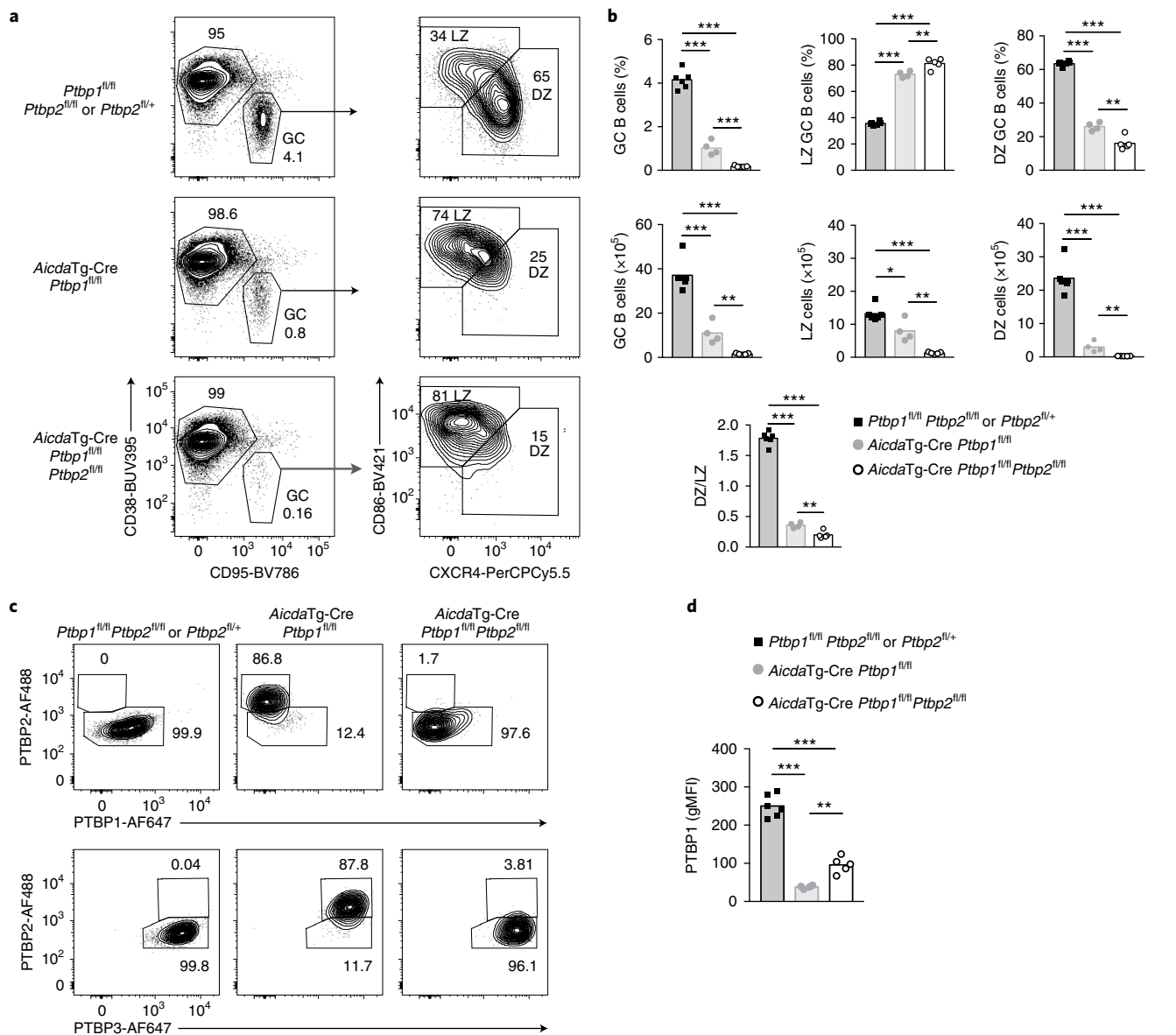


Fig. 3 | PTBP2 is partially redundant with PTBP1 in GC B cells. a, Gating strategy for GC B cells (left) and DZ and LZ GC B cells (right) from *Ptbp1^{fl/fl}Ptbp2^{fl/fl}* or *Ptbp1^{fl/fl}Ptbp2^{fl/+}* mice (top row), *AicdaTg-Cre Ptbp1^{fl/fl}* mice (middle row) and *AicdaTg-CrePtbp1^{fl/fl}Ptbp2^{fl/fl}* mice (bottom row) (genotype, left margin) on day 8 after immunization with SRBCs, pre-gated on CD19⁺ cells at left. Numbers in or adjacent to outlined areas indicate percent cells in each gate. **b**, Frequency (top row) and number (middle row) of GC B cells and DZ and LZ GC B cells in the spleen of mice as in **a** (key), identified as in **a**, and ratio of DZ GC B cells to LZ GC B cells in such mice (bottom). Each symbol represents an individual mouse; bar tops indicate the mean. * $P < 0.05$, ** $P < 0.01$ and *** $P < 0.001$ (two-tailed unpaired Student's *t*-test). **c**, Expression of PTBP1, PTBP2 and PTBP3 in GC B cells (CD95⁺CD38⁺CD19⁺) from the spleen of mice as in **a** (above plots) on 8 d after immunization with SRBCs. Numbers adjacent to outlined areas indicate percent cells in each gate. **d**, Expression of PTBP1 in GC B cells as in **c** (key), analyzed by flow cytometry and presented as the geometric mean fluorescence intensity. Each symbol represents an individual mouse. ** $P < 0.01$ and *** $P < 0.001$ (unpaired two-tailed Student's *t*-test). Data are representative of two independent experiments (**a,b**) or are from one experiment (**c,d**).

blood cells (SRBCs), the number and proportion of GC B cells was lower in *AicdaTg-CrePtbp1^{fl/fl}* (cKO) mice than in *Ptbp1^{fl/fl}Ptbp2^{fl/fl}* (control) mice, and the remaining GC B cells had the altered LZ–DZ phenotype seen in *Cd79a^{Cre/+}Ptbp1^{fl/fl}* mice (Fig. 3a,b). *AicdaTg-CrePtbp1^{fl/+}Ptbp2^{fl/+}* mice showed a number of LZ and DZ B cells similar to that of *Ptbp1^{fl/fl}Ptbp2^{fl/fl}* (control) mice (Supplementary Fig. 3k). Thus, the function of PTBP1 in B cells was required subsequent to B cell activation and expression of AID.

Considerably fewer GC B cells were detected in *AicdaTg-CrePtbp1^{fl/fl}Ptbp2^{fl/fl}* (dcKO) mice than in *Ptbp1^{fl/fl}Ptbp2^{fl/fl}* (control) or *AicdaTg-Cre Ptbp1^{fl/fl}* (cKO) mice (Fig. 3a,b and Supplementary

Fig. 3k). The residual *AicdaTg-CrePtbp1^{fl/fl}Ptbp2^{fl/fl}* (dcKO) GC B cells had the phenotype typical of LZ B cells (Fig. 3a,b), and they expressed PTBP3, had lower expression of PTBP1 than that of *Ptbp1*-sufficient GC B cells (from *Ptbp1^{fl/fl}Ptbp2^{fl/fl}* mice) but expressed no PTBP2 (Fig. 3c,d). No NP-specific IgG1-antibody-secreting cells were detected in *AicdaTg-Cre Ptbp1^{fl/fl}Ptbp2^{fl/fl}* (dcKO) mice 21 d after immunization with NP-KLH (data not shown). Thus, PTBP2, but not PTBP3, partially compensated for the loss of PTBP1.

PTBP1 regulates mRNA abundance and AS in GC B cells. We performed mRNA sequencing (mRNAseq) on LZ and DZ B cells

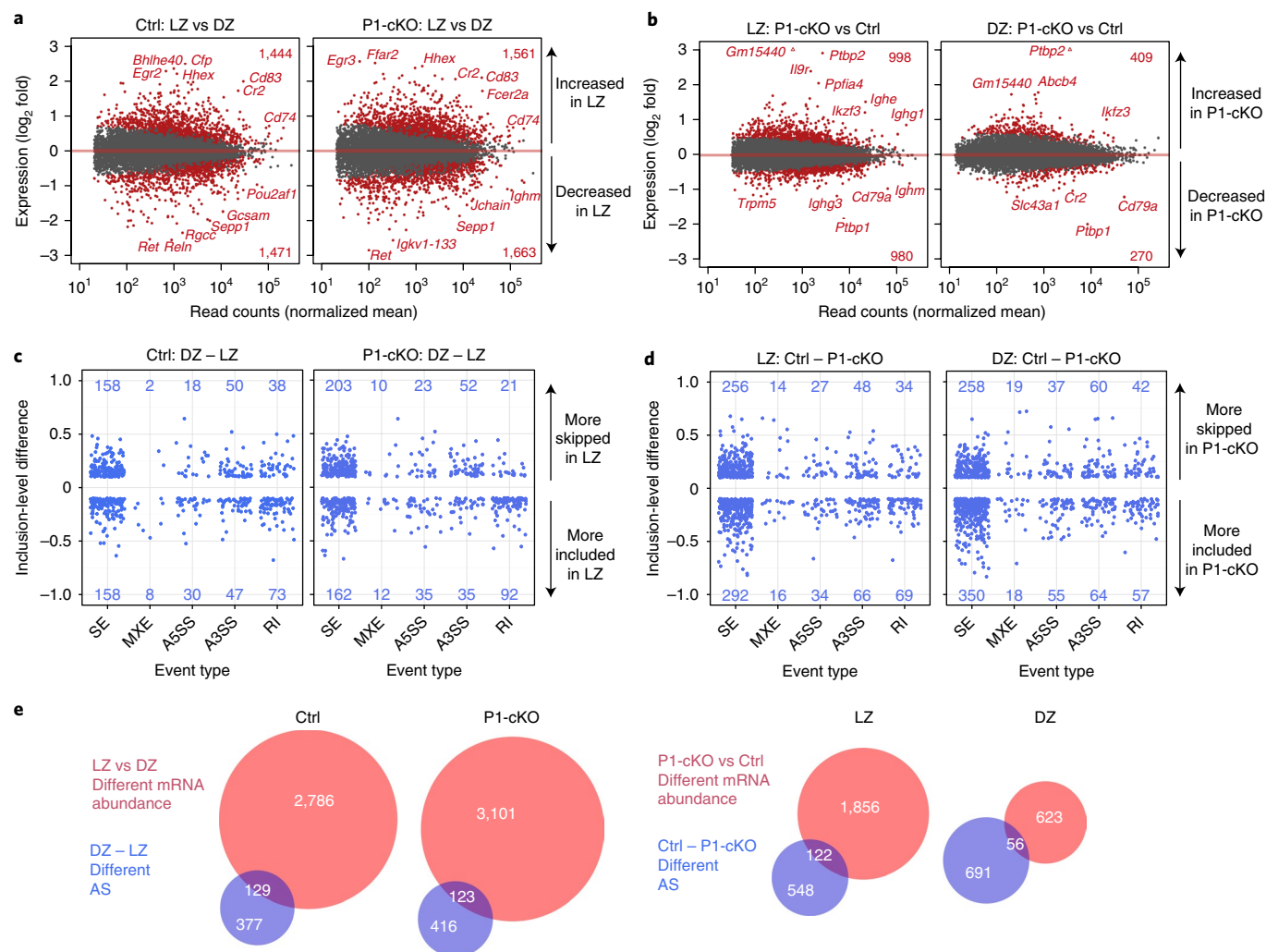


Fig. 4 | PTBP1 regulates mRNA abundance and AS in GC B cells. **a**, Change in mRNA abundance (at the gene level) in LZ GC B cells versus DZ GC B cells from *Cd79a^{+/+}Ptbp1^{fl/fl}* mice (Ctrl; left) or *Cd79a^{Cre/+}Ptbp1^{fl/fl}* mice (P1-cKO; right), presented as an MA plot of genes with at least 1 fragment per kilobase of exon per million reads mapped (FPKM) in one of the conditions analyzed: red, genes with significantly different mRNA abundance (adjusted *P* value, < 0.1); dark gray, genes with an adjusted *P* value of ≥ 0.1 . Numbers in plot (top and bottom right corners) indicate the number of genes with significantly altered mRNA abundance. **b**, Change in mRNA abundance (at the gene level) in LZ GC B cells (left) and DZ GC B cells (right) from *Cd79a^{+/+}Ptbp1^{fl/fl}* mice versus *Cd79a^{Cre/+}Ptbp1^{fl/fl}* mice (Ctrl vs P1-cKO), presented as in **a**. **c**, Change in AS of skipped exons (SE), mutually exclusive exons (MXE), alternative 5' splice sites (A5SS), alternative 3' splice sites (A3SS) and retained introns (RI) (Supplementary Fig. 4e) in LZ GC B cells versus DZ GC B cells from *Cd79a^{+/+}Ptbp1^{fl/fl}* mice (left) or *Cd79a^{Cre/+}Ptbp1^{fl/fl}* mice (right), presented as inclusion-level differences for significantly different AS events (FDR < 0.05) with an inclusion-level difference greater than 10% (≥ 0.1 or ≤ -0.1) (calculation example, Supplementary Fig. 4f). Numbers in plots indicate the number of events with significant difference. **d**, Change in AS in LZ GC B cells (left) and DZ GC B cells (right) from *Cd79a^{+/+}Ptbp1^{fl/fl}* mice versus *Cd79a^{Cre/+}Ptbp1^{fl/fl}* mice, presented as in **c**. **e**, Overlap of genes with a difference in mRNA abundance (as identified in **a,b**) and difference in AS (at any of the event types identified in **c,d**). Data are from four independent experiments with four mRNAseq libraries per condition.

from *Cd79a^{+/+}Ptbp1^{fl/fl}* (control) mice and *Cd79a^{Cre/+}Ptbp1^{fl/fl}* (PTBP1-cKO) mice. In addition, we generated a transcriptome-wide inventory of PTBP1-binding sites in mitogen-activated B cells using individual-nucleotide-resolution cross-linking and immunoprecipitation (iCLIP) (Supplementary Table 1). By combining mRNAseq with iCLIP of PTBP1, we were able to distinguish the direct effects of PTBP1 on the transcriptome from its indirect effects and, through the consideration of positional information, we were able to deduce the likely mechanism of action of PTBP1. Changes in mRNA abundance at the whole-gene level in control LZ B cells relative to those in control DZ B cells were consistent with published changes³³ and were conserved in *Ptbp1*-deficient GC B cells (Fig. 4a, Supplementary Fig. 4a,b and Supplementary Table 2).

We found 998 genes with increased mRNA abundance and 980 genes with decreased mRNA abundance in PTBP1-cKO LZ GC B cells relative to their abundance in control LZ GC B cells, and 409 genes with increased mRNA abundance and 270 genes with decreased mRNA abundance in PTBP1-cKO DZ GC B cells relative to their abundance in control DZ GC B cells (Fig. 4b and Supplementary Table 2). The changes in genes that were expressed differentially in LZ B cells and DZ B cells due to deletion of *Ptbp1* showed a strong positive correlation (Supplementary Fig. 4c), which indicated that the absence of PTBP1 affected the same genes in LZ B cells that it affected in DZ B cells. PTBP1 can increase mRNA stability when bound to 3' untranslated regions (UTRs)^{19,23}. Among genes with either increased mRNA abundance or decreased mRNA abundance, the proportion of genes bound by PTBP1 in

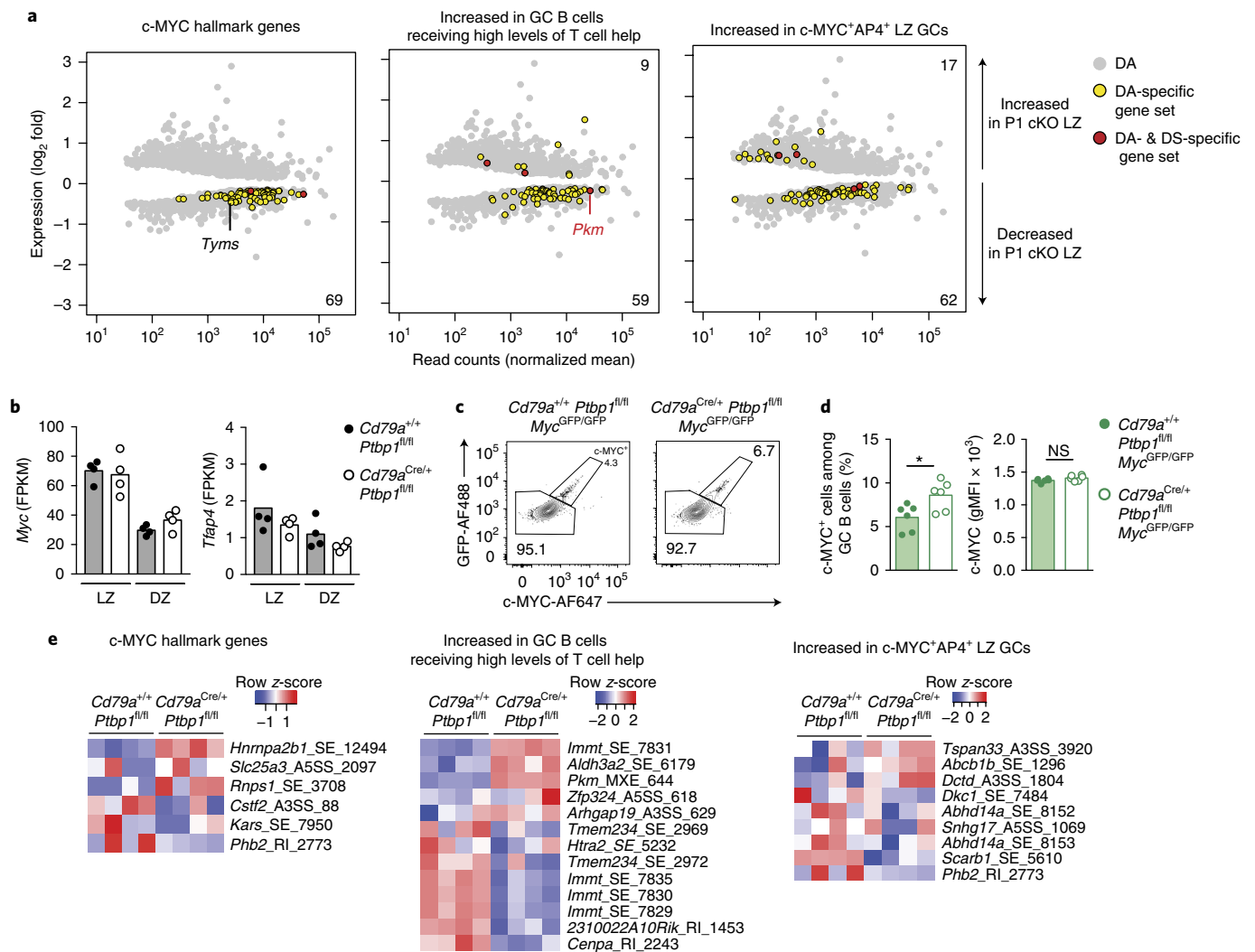


Fig. 5 | The positive-selection gene-expression program is reduced after deletion of *Ptbp1*. **a**, Genes with different mRNA abundance (DA) in LZ GC B cells due to deletion of *Ptbp1*, assessed for the following gene sets: targets of c-MYC (GSEA HALLMARK_MYC_TARGETS_V1) (left), genes with higher expression in GC B cells receiving high levels of T cell help than in those not receiving high levels of T cell help (middle), and genes with higher expression in c-MYC⁺AP4⁺ LZ GC B cells than in c-MYC⁺AP4⁻ LZ GC B cells (right), presented as MA plots. DS, genes with different AS (inclusion-level difference > 10%). Numbers in plots (top and bottom right corners) indicate the number of genes that are part of the gene sets studied and have different mRNA abundance in LZ GC B cells due to the lack of PTBP1. DA (light gray), genes with different mRNA abundance in LZ GC B cells due to deletion of *Ptbp1*; DA-specific gene set (yellow), genes with different mRNA abundance in LZ GC B cells due to deletion of *Ptbp1* that were part of the specified gene sets; DA- & DS-specific gene set (red), genes with different mRNA abundance and also different AS in LZ GC B cells due to deletion of *Ptbp1* that were part of the specified gene sets. **b**, mRNAseq analysis of *Myc* and *Ttp44* (which encodes AP4) in *Cd79a*^{+/+}*Ptbp1*^{fl/fl} and *Cd79a*^{Cre/+}*Ptbp1*^{fl/fl} (key) LZ and DZ GC B cells (below plot). **c**, Gating strategy for identifying GFP-c-MYC⁺ GC B cells (CD19⁺CD38^{lo}CD95^{hi}) among splenocytes from *Rag2*^{-/-} mice reconstituted with *Cd79a*^{+/+} *Ptbp1*^{fl/fl} *Myc*^{GFP/GFP} or *Cd79a*^{Cre/+} *Ptbp1*^{fl/fl} *Myc*^{GFP/GFP} bone marrow cells (above plots), immunized with SRBCs and analyzed 8 d after immunization. Numbers adjacent to outlined areas indicate percent cells in each gate. **d**, Frequency of GFP-c-MYC⁺ cells among GC B cells as in **c** (left) and geometric mean fluorescence intensity of c-MYC in GFP-c-MYC⁺ GC B cells as in **c** (right). Each symbol represents an individual mouse; bar tops indicate the mean. NS, not significant ($P > 0.05$); * $P < 0.05$ (unpaired two-tailed Student's *t*-test). **e**, Differential AS events (FDR < 0.05) with an inclusion-level difference greater than 10% due to *Ptbp1* deletion in LZ GC B cells, assessed for genes in sets as in **a** (above plots); right margin, gene symbol, followed by the type of AS event (as in Fig. 4c) and the rMATS identification number (Supplementary Table 3; genes bound by PTBP1 near the AS event, Supplementary Table 5). Data are from four independent experiments with four mRNAseq libraries per condition (**a,b,e**) or are representative of one experiment (**c,d**).

their 3' UTRs was similar (~20%, Supplementary Fig. 4d). Thus, binding of PTBP1 to 3' UTRs did not seem to have a substantial 'preference' toward increasing mRNA stability or decreasing it in GC B cells.

We used the rMATS computational tool (for the detection of differential AS) to determine inclusion-level differences between any two conditions for five different types of AS events (Supplementary Fig. 4e,f). We identified 266 AS events that were more skipped in

control LZ B cells than in control DZ B cells and 316 AS events that were more included in control LZ B cells than in control DZ B cells (all from 506 genes), with an inclusion-level difference greater than 10% (Fig. 4c and Supplementary Table 3); this indicated extensive changes in AS in the transition between LZ and DZ. The changes in AS due to *Ptbp1* deficiency were greater in both the magnitude of events and the number of events (Fig. 4d, 856 AS events in LZ GC B cells and 960 AS events in DZ GC B cells) than the differences noted

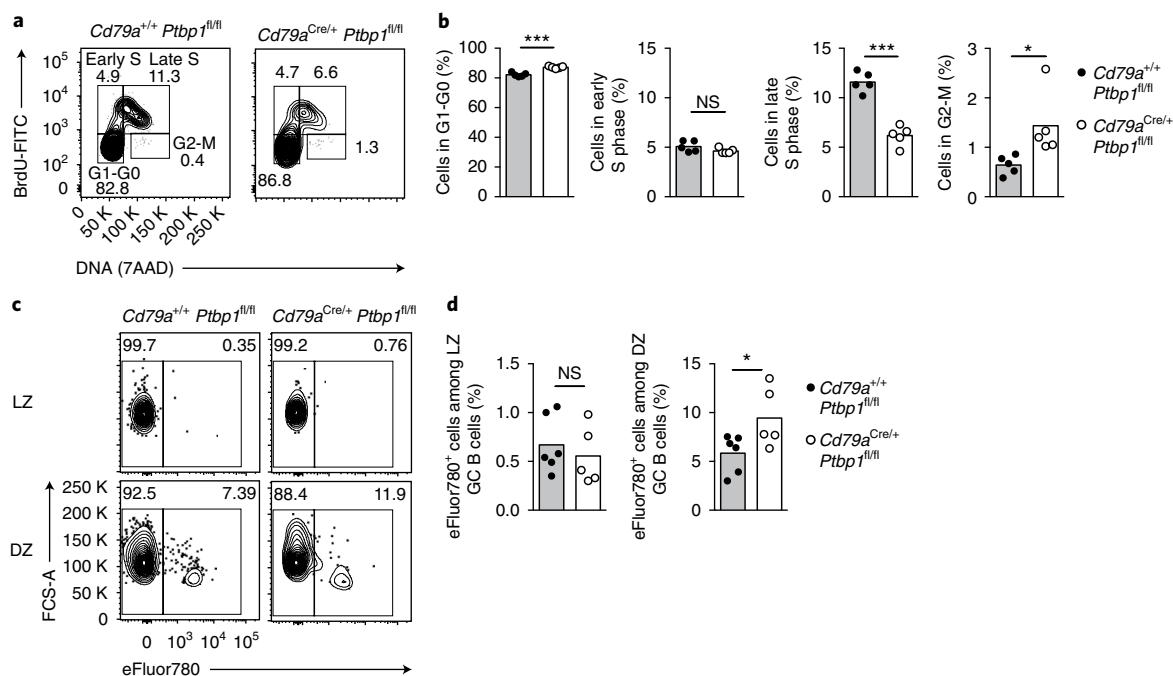


Fig. 6 | Late S-phase progression is impaired in the absence of PTBP1. **a**, Gating strategy for GC B cells (B220⁺CD19⁺CD38^{lo}CD95^{hi}) at various stages of the cell cycle among splenocytes from *Cd79a*^{+/+}*Ptbp1*^{fl/fl} and *Cd79a*^{Cre/+}*Ptbp1*^{fl/fl} mice (above plots) 7 d after immunization with NP-KLH, assessed by flow cytometry on the basis of staining of BrdU and with the membrane-impermeable DNA-intercalating dye 7-AAD. Numbers adjacent to outlined areas indicate percent cells in each phase. **b**, Frequency of cells in each phase of the cell cycle as in **a**. NS, not significant ($P > 0.05$); * $P < 0.05$ and *** $P < 0.001$ (two-tailed unpaired Student's *t*-test). **c**, Gating strategy for the flow-cytometry analysis of dead cells (with the viability dye eFluor780) among LZ (CD86^{hi}CXCR4^{lo}) or DZ (CD86^{lo}CXCR4^{hi}) GC B cells (CD95⁺CD38^{lo}CD19⁺B220⁺) from *Cd79a*^{+/+}*Ptbp1*^{fl/fl} and *Cd79a*^{Cre/+}*Ptbp1*^{fl/fl} mice (above plots). Numbers adjacent to outlined areas indicate percent eFluor780⁻ (live) cells (left) or eFluor780⁺ (dead) cells (right). **d**, Frequency of dead (eFluor780⁺) cells in mice as in **c** (key). NS, not significant ($P > 0.05$); * $P < 0.05$ (two-tailed unpaired *t*-test). Each symbol (**b,d**) represents an individual mouse; bar tops indicate the mean. Data are representative of two mice (**a,c**) or are from one experiment representative of three independent experiments with similar results (**b,d**).

for control LZ GC B cells versus control DZ GC B cells (Fig. 4c, 582 events). The 52% overlap of AS events that were different in control LZ B cells versus control DZ B cells and those affected by *Ptbp1* deletion (Supplementary Fig. 4g) indicated that PTBP1 affected a substantial proportion of the AS events that differed in LZ B cells versus DZ B cells.

379 AS events were more skipped and 477 AS events were more included (in 670 genes) in PTBP1-cKO LZ B cells than in control LZ B cells (Fig. 4d and Supplementary Table 3). 416 AS events were more skipped and 544 AS events were more included (in 747 genes) in PTBP1-cKO DZ B cells than in control DZ B cells (Fig. 4d and Supplementary Table 3). The proportion of AS events directly regulated by PTBP1, inferred from the binding of PTBP1 in the vicinity of the event, varied depending on the type of AS event and ranged from ~50% in mutually exclusive exons to ~7% in alternative 3' splice sites (Supplementary Fig. 4h). Among AS events more skipped or more included in PTBP1-cKO B cells than in control B cells, the proportion of events that were bound in their vicinity by PTBP1 in our PTBP1 iCLIP data was similar (Supplementary Fig. 4h), which indicated that PTBP1 both repressed AS and activated AS in GC B cells. The overlap between genes with different mRNA abundance and those with different AS due to deletion of *Ptbp1* was 6% in the LZ and in 8% the DZ (Fig. 4e). Similarly, there was a small overlap between genes with changes in abundance and AS in the comparison of *Cd79a*^{+/+}*Ptbp1*^{fl/fl} (control) LZ B cells versus control *Cd79a*^{+/+}*Ptbp1*^{fl/fl} (control) DZ B cells (Fig. 4e). Together our data identified PTBP1 as a post-transcriptional regulator in GC B cells, in which it controlled mRNA abundance and five different types of AS events.

PTBP1 is necessary for the c-MYC-dependent program induced after positive selection. To determine if PTBP1 regulated changes in annotated gene-ontology (GO) pathways, we assessed genes with changes at the level of mRNA abundance or AS due to *Ptbp1* deletion separately. Several GO terms relevant to the biology of GC B cells showed enrichment for genes with a difference in mRNA abundance due to deletion of *Ptbp1* (Supplementary Fig. 5 and Supplementary Table 4). No pathways showed enrichment (false-discovery rate (FDR), <0.1) when AS changes were analyzed (Supplementary Table 4). Instead, individual genes of different pathways were regulated by PTBP1 at the level of AS.

Pathways involved in nucleotide biosynthesis and cell proliferation (Supplementary Fig. 5a–c) showed enrichment for genes with differential mRNA abundance in LZ B cells and DZ B cells due to the lack of PTBP1. In LZ B cells, most of the differentially expressed genes within these pathways had decreased mRNA abundance (Supplementary Fig. 5b). LZ B cells showed enrichment for The Ras protein signaling pathway was also enrichment in LZ B cells with genes that had different mRNA abundance, but most of these genes had increased mRNA abundance due to the lack of PTBP1 (Supplementary Fig. 5b). Pathways linked to B cell differentiation, lymphocyte migration, cholesterol metabolism and the regulation of apoptosis in leukocytes (Supplementary Fig. 5a,c) showed enrichment for genes with different mRNA abundance in DZ B cells due to deletion of *Ptbp1*. Among the 243 genes with different mRNA abundance that belonged to the enriched pathways, we found that 64 were bound by PTBP1 in their 3' UTR and only 10 had AS in the absence of PTBP1 (Supplementary Fig. 5b,c). Thus, PTBP1 directly regulated some of these genes but also had

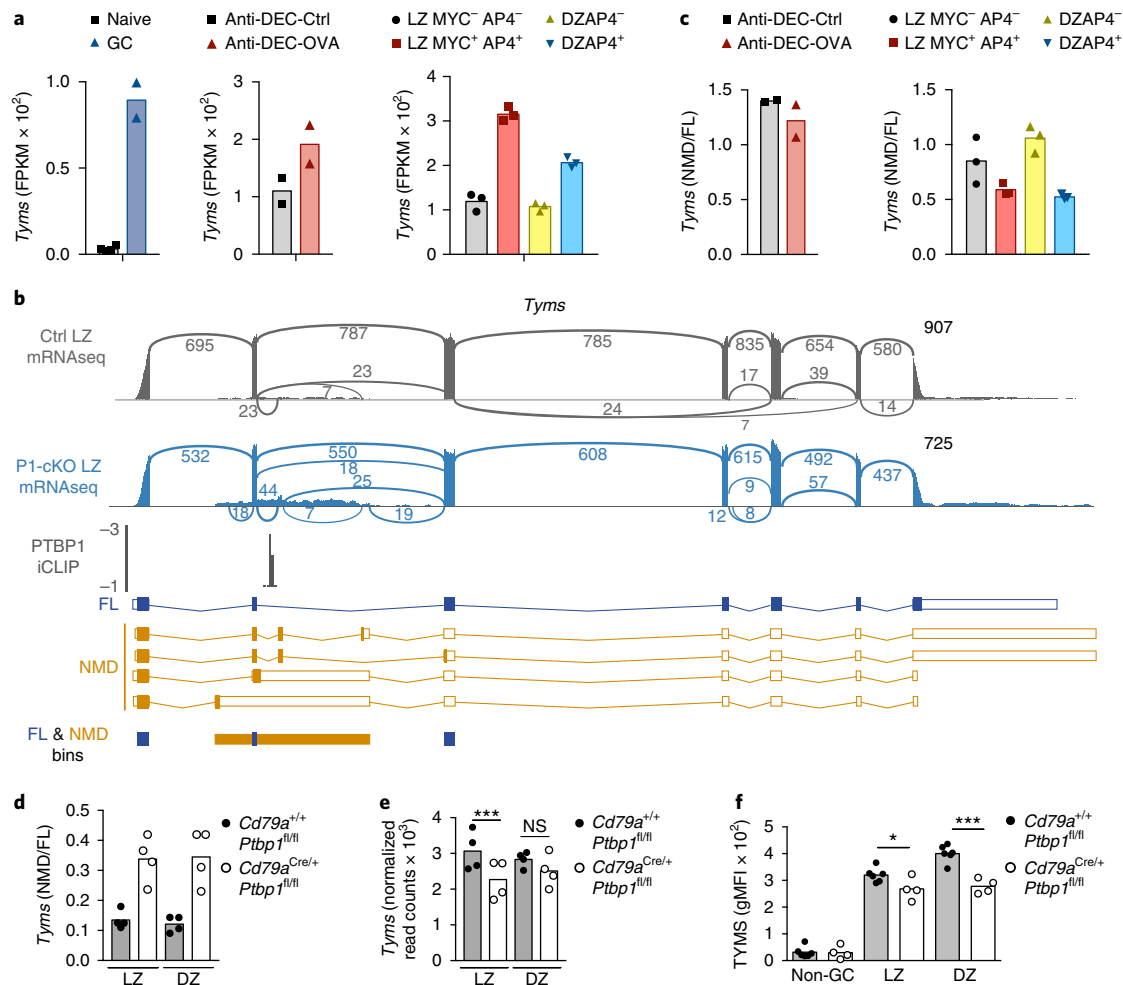


Fig. 7 | PTBPI regulates the abundance of *Tyms* mRNA through control of AS. **a, Expression of *Tyms* (FPKM) in GC B cells and naive B cells⁴⁹ (left), in GC B cells receiving high levels of T cell help (Anti-DEC-Ctrl) or not (Anti-DEC-OVA)³ (middle), or in LZ and DZ B cells expressing c-MYC and AP4 or not⁷ (right). **b**, mRNAseq analysis of *Tyms* in *Cd79a*^{+/+}*Ptbp1*^{fl/fl} (Ctrl) and *Cd79a*^{Cre/+}*Ptbp1*^{fl/fl} (PI-cKO) LZ GC B cells (top two rows), presented as ‘sashimi plots’ showing read coverage and reads that map to exon-exon junctions (arches; numbers indicate reads that map to that junction), and iCLIP analysis of PTBPI (below); scale bar (bottom), number of independent X-link sites (PTBPI-binding sites) identified. **c**, Ratio of NMD reads (mapping to exons and retained introns that would generate an NMD *Tyms* transcript; yellow bins in **b**) to FL reads (mapping to the first three exons needed for the full-length *Tyms* transcript; blue bins in **b**) (NMD/FL) for mRNAseq libraries from GC B cells receiving high levels of T cell help or not (left) and in LZ and DZ GC B cells expressing c-MYC and AP4 or not (right) (as in **a**). **d**, Ratio of NMD reads to FL reads for mRNAseq libraries from *Cd79a*^{+/+}*Ptbp1*^{fl/fl} and *Cd79a*^{Cre/+}*Ptbp1*^{fl/fl} (key) LZ and DZ GC B cells (below plot). **e**, Expression of *Tyms* mRNA in cells as in **d**, presented as DESeq2-normalized read counts. NS, not significant (adjusted *P* value > 0.1 (DESeq2)); ****P* < 0.001 (DESeq2; adjusted *P* value). **f**, Flow-cytometry analysis of TYMS in non-GC B cells (CD19⁺CD95⁻CD38^{hi}) and in LZ cells (CD86^{hi}CXCR4^{lo}) or DZ cells (CD86^{lo}CXCR4^{hi}) among GC B cells (CD19⁺CD95⁺CD38^{lo}) from the spleen of mice 8 d after immunization with SRBCs. **P* < 0.05 and ****P* < 0.001 (Student’s two-tailed *t*-test). Each symbol (**a-c-f**) represents an individual mRNAseq library (**a-c-e**) or mouse (**f**); bar tops indicate the mean. Data are representative of four independent experiments with two (**b**) or four (**d,e**) mRNAseq libraries per condition (**b,d,e**) or are from one experiment (**f**).**

an indirect effect on the expression of genes in these pathways. We investigated further how the lack of PTBPI affected the expression of genes that are part of the c-MYC hallmark³⁴ and also of genes induced in response to T cell help^{3,7}. In LZ B cells lacking PTBPI, there was a globally lower mRNA abundance of the genes induced after positive selection relative to the mRNA abundance of such genes in *Cd79a*^{+/+}*Ptbp1*^{fl/fl} (control) LZ B cells (Fig. 5a). 21% of the genes with lower mRNA abundance in LZ B cells due to deletion of *Ptbp1* were part of the gene-expression program induced after positive selection (Supplementary Fig. 6a and Supplementary Table 5).

The abundance of *Myc* mRNA and its AS pattern were the same in *Cd79a*^{Cre/+}*Ptbp1*^{fl/fl} (cKO) LZ B cells and *Cd79a*^{+/+}*Ptbp1*^{fl/fl} (control) LZ B cells (Fig. 5b and Supplementary Table 3). We recon-

stituted *Rag2*^{-/-} mice (which have a congenital deficiency in mature B cells and T cells) with *Cd79a*^{Cre/+}*Ptbp1*^{fl/fl}*Myc*^{GFP/GFP} bone marrow cells or *Cd79a*^{+/+}*Ptbp1*^{fl/fl}*Myc*^{GFP/GFP} bone marrow cells and immunized the resultant mice with SRBCs and found that the proportion of GFP-c-MYC⁺ cells among GC B cells and the level of c-MYC protein was similar in each group of mice (Fig. 5c,d). Furthermore, the abundance of *Tfap4* mRNA, which encodes AP4 (Fig. 5b), and the phosphorylation of ribosomal protein S6 at Ser240 and Ser244 (Supplementary Fig. 6b) in *Cd79a*^{Cre/+}*Ptbp1*^{fl/fl} (cKO) LZ GC B cells was similar to that in *Cd79a*^{+/+}*Ptbp1*^{fl/fl} (control) LZ GC B cells. Additionally, *Cxcr4* and *Cxcr5* (which encode chemokine receptors), *Bcl6*, *Bach2*, *Foxo1* and *Batf* (which encode transcription factors), *Aicda* (which encodes AID) and *Il21r* (which

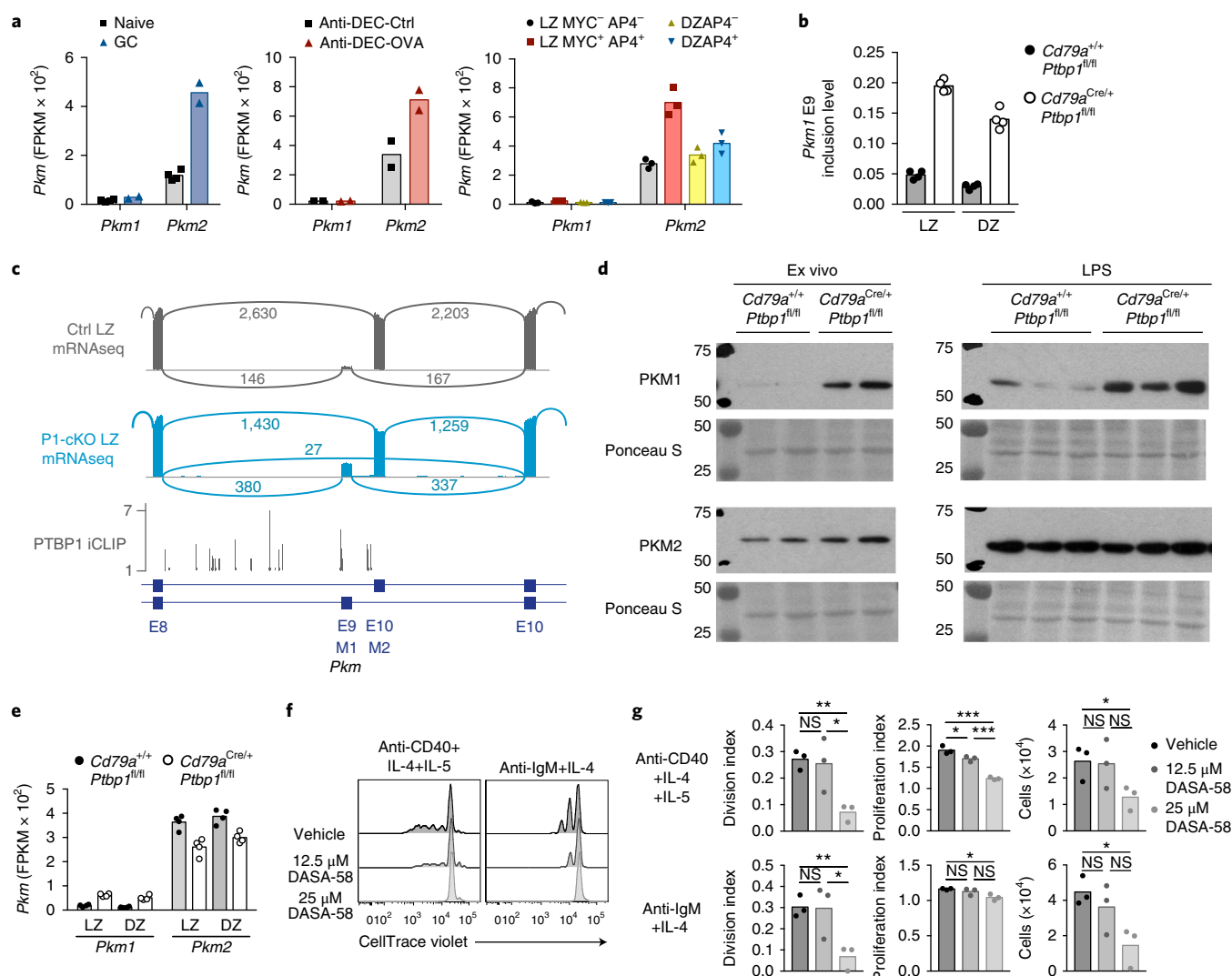


Fig. 8 | PTBP1 regulates AS of *Pkm*. **a**, Abundance of *Pkm1* and *Pkm2* transcripts (FPKM) in GC B cells and naive B cells (left), in GC B cells receiving high levels of T cell help or not (middle) or in LZ and DZ GC B cells expressing *c-MYC* and AP4 or not (right) (as in Fig. 7a), calculated with the Cuffnorm program of Cufflinks software. **b**, rMATS inclusion values for exon 9 of *Pkm* (*Pkm1* E9) in LZ and DZ cells (below plot) from *Cd79a*^{+/+}*Ptbp1*^{fl/fl} and *Cd79a*^{Cre/+}*Ptbp1*^{fl/fl} mice (key). **c**, mRNAseq analysis of *Pkm* exons 8–10 in *Cd79a*^{+/+}*Ptbp1*^{fl/fl} and *Cd79a*^{Cre/+}*Ptbp1*^{fl/fl} LZ GC B cells (top two rows), and iCLIP analysis of PTBP1 (presented as in Fig. 7b). **d**, Immunoblot analysis of PKM1 and PKM2 in lysates of B cells freshly isolated from the spleen of *Cd79a*^{+/+}*Ptbp1*^{fl/fl} and *Cd79a*^{Cre/+}*Ptbp1*^{fl/fl} mice (above plots; one mouse per lane), and analyzed without further treatment (Ex vivo; left) or stimulated in vitro for 48 h with lipopolysaccharide (LPS; right), presented along with Ponceau S staining of the blots (cropped images; full images, Supplementary Fig. 8). Left margin, size (in kilodaltons). **e**, *Pkm1* and *Pkm2* transcripts (FPKM) in our mRNAseq libraries from *Cd79a*^{+/+}*Ptbp1*^{fl/fl} and *Cd79a*^{Cre/+}*Ptbp1*^{fl/fl} (key) LZ and DZ GC B cells (below plots), calculated with Cuffnorm. **f**, CellTrace Violet profiles of splenic B cells stimulated in vitro for 62 h with antibody to (Anti-) CD40 plus IL-4 and IL-5 or with antibody to IgM plus IL-4 (above plots) in the presence of DASA-58 or vehicle (DMSO, in the same amount as that used for 50 μ M DASA-58). **g**, Quantification of the proliferation profiles in **f** (left and middle) and absolute number of cells recovered from the cultures (right). NS, not significant ($P > 0.05$); * $P < 0.05$, ** $P < 0.01$ and *** $P < 0.001$ (unpaired Student's two-tailed *t*-test). Each symbol (**a, b, e, g**) represents an individual mRNAseq library (**a, b, e**) or mouse (**g**); bar tops indicate the mean. Data are from four independent experiments with four (**b, e**) or two (**c**) mRNAseq libraries per condition (**b, c, e**) or are from one experiment with several mice (**d, f, g**).

encodes a cytokine receptor) had equivalent expression and AS patterns in *Ptbp1*-deficient and *Cd79a*^{+/+}*Ptbp1*^{fl/fl} (control) GC B cells (Supplementary Fig. 6c–e and Supplementary Table 3). Thus GC B cells do not require PTBP1 for the sensing of T cell help or the induced expression of *c-MYC*.

28% of the mRNAs that were part of the *c-MYC*-dependent gene-expression program induced after positive selection and that were decreased in LZ B cells due to *Ptbp1* deletion were bound by PTBP1 in their 3' UTR (Supplementary Fig. 6a and Supplementary Table 5). This indicated a direct role for PTBP1 in stabilizing a

fraction, but not all, of *c-MYC*-dependent transcripts. Moreover, 22 genes that were induced after positive selection showed differential AS (inclusion-level difference > 10%) in *Ptbp1*-deficient LZ B cells relative to their AS in *Cd79a*^{+/+}*Ptbp1*^{fl/fl} (control) LZ B cells (Fig. 5e and Supplementary Fig. 6a), and six of these were bound by PTBP1 near the AS event (Supplementary Table 5). *Pkm* (which encodes pyruvate kinase), *Abcb1b* (which encodes an ATP-binding-cassette transporter), *Tspan33* (which encodes a tetraspanin protein), *Phb2* (which encodes the repressor Bcap37) and *Dkc1* (which encodes the dyskerin pseudouridine synthase DKC1) were the only genes with

both decreased mRNA abundance and differential AS (inclusion-level difference > 10%) due to the lack of PTBP1. Thus, PTBP1 regulated expression of the c-MYC-dependent gene-expression program both directly and indirectly in positively selected GC B cells by regulating mRNA abundance and AS.

PTBP1 regulates the proliferation of GC B cells. We investigated whether PTBP1 was required for GC B cell proliferation by measuring DNA content and incorporation of the thymidine analog bromodeoxyuridine (BrdU) into GC B cells in vivo. The proportion of *Cd79a^{Cre/+}Ptbp1^{fl/fl}* (cKO) GC B cells in late S phase (BrdU⁺ with high DNA content) was lower than that of *Cd79a^{+/+}Ptbp1^{fl/fl}* (control) GC B cells in late S phase, in mice immunized with NP-KLH (Fig. 6a,b). In contrast, the proportion of cells that were in early S phase (BrdU⁺ with low DNA content) was similar among *Cd79a^{Cre/+}Ptbp1^{fl/fl}* (cKO) GC B cells and *Cd79a^{+/+}Ptbp1^{fl/fl}* (control) GC B cells. Additionally, *Cd79a^{Cre/+}Ptbp1^{fl/fl}* (cKO) GC B cell populations had a greater proportion of cells in G2 and M phases than did *Cd79a^{+/+}Ptbp1^{fl/fl}* (control) GC B cell populations (Fig. 6a,b). The proportion of cells in late S phase was lower among both LZ B cells (in five of five experiments) and DZ B cells (in four of five experiments) from *Cd79a^{Cre/+}Ptbp1^{fl/fl}* (cKO) mice than among those from *Cd79a^{+/+}Ptbp1^{fl/fl}* (control) mice (Supplementary Fig. 7a). We also observed a lower proportion of cells in late S phase among GC B cells from *AicdaTg-CrePtbp1^{fl/fl}* (cKO) mice than among those from *AicdaTg-CrePtbp1^{+/+}Ptbp2^{+/+}* or *Ptbp1^{fl/fl}Ptbp2^{fl/fl}* mice, after immunization with SRBCs (Supplementary Fig. 7b). The proportion of GC B cells in late S phase was also lower among CD45.2⁺ *Ptbp1*-deficient cells than among CD45.2⁺ *Ptbp1*-sufficient cells from B6.SJL competitive chimeras reconstituted with a 1:1 mixture of bone marrow cells from CD45.1⁺ B6.SJL mice and CD45.2⁺ *Cd79a^{Cre/+}Ptbp1^{fl/fl}* (cKO) mice or from CD45.1⁺ B6.SJL mice and CD45.2⁺ *Cd79a^{+/+}Ptbp1^{fl/fl}* (control) mice and then immunized with NP-KLH (Supplementary Fig. 7c), which showed that this was a cell-autonomous defect. In contrast to results obtained for GC B cells, the proportion of cells at different stages of the cell cycle was normal among the highly proliferative early-pre B cells of *Cd79a^{Cre/+}Ptbp1^{fl/fl}* (cKO) mice (Supplementary Fig. 7d). Thus, PTBP1 was not universally required in cells that were undergoing cell division but was necessary for the progression of GC B cells through late S phase.

Closer analysis of the expression of genes encoding molecules important for progression through the cell cycle revealed that the expression of *Ccnd2*, *Ccnd3* and *Ccne2* was unaffected in *Cd79a^{Cre/+}Ptbp1^{fl/fl}* (cKO) GC B cells relative to such expression in *Cd79a^{+/+}Ptbp1^{fl/fl}* (control) GC B cells (Supplementary Fig. 7e), which suggested that the enrichment for proliferation and nucleotide-biosynthetic GO pathways did not arise from a failure to express early cell-cycle-progression factors. Impaired nucleotide synthesis could cause replication stress as cells progress through S phase and could cause cell death³⁵. Flow cytometry using a fixable viability dye to detect non-viable cells showed a higher proportion of dead cells among *Cd79a^{Cre/+}Ptbp1^{fl/fl}* DZ GC B cells than among *Cd79a^{+/+}Ptbp1^{fl/fl}* DZ GC B cells (Fig. 6c,d). In contrast, the proportion of dead cells among LZ B cells were similar for *Ptbp1*-deficient cells and *Ptbp1*-sufficient cells (Fig. 6c,d). Thus, PTBP1 was necessary for progression through the S and G2-M phases of the cell cycle and promoted the survival of DZ cells.

PTBP1 controls AS of c-Myc-dependent genes that encode molecules important for proliferation. Given the impaired proliferation of *Ptbp1*-deficient GC B cells, we looked for evidence of PTBP1-dependent AS isoforms among genes that were part of the c-MYC-dependent gene-expression program and encoded molecules important for proliferation. mRNA from the gene encoding thymidylate synthase (*Tyms*, a target of c-MYC; Fig. 5a), which is necessary for de novo nucleotide synthesis, was 30-fold greater in

abundance in GC B cells than in naive B cells and increased after positive selection in GC B cells (Fig. 7a). *Tyms* mRNA was spliced differently in the absence of PTBP1 (Fig. 7b). Deletion of *Ptbp1* resulted in a complex AS pattern, with increased inclusion of exons and retained introns (yellow bins, Fig. 7b) that generated transcript isoforms predicted to be degraded by NMD. We quantified the ratio of mRNAseq reads that mapped to segments generating transcripts predicted to be degraded by NMD ('NMD reads'; yellow bins, Fig. 7b) to mRNAseq reads that mapped to the first three exons of *Tyms*, which encode the full-length (FL) protein ('FL reads'; blue bins, Fig. 7b). The ratio of NMD reads to FL reads was reduced after positive selection in GC B cells (Fig. 7c), which indicated an increase in protein-coding *Tyms* mRNA in positively selected GC B cells. The ratio of NMD reads to FL reads was higher in *Ptbp1*-deficient LZ and DZ B cells than in *Ptbp1*-sufficient LZ and DZ B cells (Fig. 7d). The abundance of *Tyms* mRNA (at the whole-gene level) was reduced due to deletion of *Ptbp1* in LZ B cells (Fig. 7e). TYMS protein was decreased in abundance due to deletion *Ptbp1* in LZ and DZ B cells (Fig. 7f). Consistent with a direct role for PTBP1 in regulating those *Tyms* AS events, iCLIP analysis showed PTBP1 bound to the AS region of *Tyms* (Fig. 7b). These data indicated that PTBP1 ensured increased expression of TYMS during positive selection by regulating AS of *Tyms*.

The pyruvate kinase PKM catalyzes the conversion of phosphoenolpyruvate to pyruvate in glycolysis and is also encoded by a target of c-MYC²⁸ that was spliced differentially due to deletion of *Ptbp1* (Fig. 5e). *Pkm* encodes two protein isoforms generated from mutually exclusive inclusion of exon 9 (PKM1) or exon 10 (PKM2). Whereas PKM1 exists only as a highly active tetrameric form, PKM2 interchanges among less-active monomeric and dimeric forms as well as a fully active tetramer in response to nutrient availability and energy demands³⁶. B cells expressed *Pkm2* almost exclusively, and *Pkm2* was induced after positive selection in GC B cells, but *Pkm1* was not (Fig. 8a). In the absence of PTBP1, the inclusion level of exon 9 increased from 0.05 to 0.2 (Fig. 8b,c). Immunoblot analysis of proteins from naive and mitogen-activated B cells in vitro revealed that PKM1 was hardly detected in *Cd79a^{+/+}Ptbp1^{fl/fl}* B cells but was readily detected in *Cd79a^{Cre/+}Ptbp1^{fl/fl}* (cKO) B cells (Fig. 8d). This AS event has been shown to be regulated by PTBP1 in human cell lines to favor the production of PKM2^{28,31}. Our iCLIP data revealed binding of PTBP1 close to the intronic 3' splice site of *Pkm* exon 9 in B cells (Fig. 8c). Thus, PTBP1 promoted skipping of this exon in favor of the inclusion of exon 10 and suppression of *Pkm1* mRNA in GC B cells (Fig. 8e).

Expression of PKM1 has been shown to impair the proliferation of malignant cells and non-transformed fibroblasts, and the small molecule DASA-58 activates the tetramerization of PKM2 and inhibits the proliferation of transformed cells³⁶. DASA-58 reduced the proliferation of mouse B cells in response to in vitro stimulation with antibody to the costimulatory receptor CD40 plus the cytokines IL-4 and IL-5 or stimulation with antibody to IgM plus IL-4 (Fig. 8f,g). These findings were consistent with the hypothesis that increased activity of pyruvate kinase, as would be expected after PKM1 expression, is detrimental for B cell proliferation.

Discussion

PTBP1 is either induced by and acts downstream of c-MYC or forms part of a previously unrecognized pathway that acts in parallel with c-MYC to drive GC B cell proliferation. We favor the former hypothesis, as there is evidence that PTBP1 is encoded by a c-MYC-responsive gene in other cell systems^{28,29}. A proliferation defect of *Ptbp1*-deficient embryonic stem cells and human CD4⁺ T cells with reduced levels of PTBP1 has been observed^{30,37,38}, which indicates that PTBP1 is necessary for cell proliferation in other systems, although the basis for the reported effects is not clear. However, the requirement for PTBP1 in proliferation is not universal, as the

proliferation of *Ptbp1*-deficient early pre-B cells was normal. This difference could reflect compensatory mechanisms or the distinct environment of the GC versus that of the bone marrow^{39,40}.

PTBP1 controlled gene expression by regulating multiple processes in the biogenesis and fate of mRNA. The mRNA abundance or AS of 213 genes that were part of the c-MYC-dependent gene-expression program induced after positive selection was PTBP1 dependent, but there were additional direct and indirect targets of PTBP1 that were not part of the MYC-dependent program. Among those, we observed changes in the AS of *Sema4d*, *Pdlim7*, *Pbrm1*, *Acly* and *Ikzf3*. Changes in semaphorin 4d (CD100; encoded by *Sema4d*) could affect the migration of GC B cells through the LZ and DZ and interactions with T cells⁴¹. Changes in enigma (encoded by *Pdlim7*) could alter expression of the tumor suppressor p53⁴². Altered splicing of the gene encoding ATP citrate lyase (*Acly*) could have an effect on lipid biosynthesis⁴³. Polybromo-1 (BAF180; encoded by *Pbrm1*) is part of the SWI-SNF-B (PBAF) chromatin-remodeling complex and is a cofactor of c-MYC that might help propagate the c-MYC-induced gene-expression program⁴⁴, and alterations in Aiolos (encoded by *Ikzf3*) might influence plasma cell formation⁴⁵. Despite the potential for molecules encoded by these genes to have roles in GC B cell biology, most of the alternative isoforms found have not been studied before, to our knowledge. Elucidation of the functions of molecules encoded by these AS transcripts in GC B cell biology will require careful investigation.

Pkm and *Tyms* are but two examples of c-MYC-regulated genes that are subject to PTBP1-dependent AS. Inhibition of TYMS by 5-fluorouracil blocks the proliferation of primary T cells⁴⁶ and B cells in vitro (data not shown). Splicing of the retained intron upstream of exon 2 from the full-length *Tyms* transcript is necessary for increased *Tyms* mRNA expression in cultured cells⁴⁷. Reduced amounts of TYMS could be one limiting factor for the proliferation of positively selected GC B cells. Other events regulated by PTBP1 must also promote GC B cell proliferation, and our results indicate that the regulation of PKM activity is important for B cell proliferation. PTBP1, by regulating the AS of *Pkm*, might limit glycolytic flux and thereby contribute to biosynthetic pathways through the accumulation of glycolytic intermediates³⁶. Consistent with that, PKM1 is growth inhibitory when it is expressed in cancer xenograft tumor models³⁶, and B cell proliferation in vitro was inhibited by activators of PKM2.

Published studies have reported a function for PTBP2 in antibody class-switch recombination⁴⁸. We did not detect PTBP2 expression in GC B cells unless *Ptbp1* was deleted, and secretion of antigen-specific IgG1 was unaffected in mice with *Ptbp2*-deficient B cells. Therefore, it is unlikely that PTBP2 promotes class-switch recombination in GC B cells. Nonetheless, the increase in the frequency of IgG1⁺ GC B cells among *Ptbp1*-deficient GC B cells might indicate that, if expressed, PTBP2 might indeed promote antibody class-switch recombination.

There might be additional PTBP1-mediated post-transcriptional processes of importance to the GC reaction. Changes in APA analyzed with the DaPars tool found that deletion of *Ptbp1* affected the APA of four genes in LZ B cells and seven genes in DZ B cells (data not shown), suggestive of a more limited role for PTBP1 in regulating APA in GC B cells than its roles controlling AS and mRNA abundance. However, full elucidation of the roles of PTBP1 in APA will require analysis of RNA-based next-generation sequencing libraries specifically targeted at capturing 3' ends. In the present study, we were unable to measure the effect of PTBP1 on the tempo of translation, such as through internal-ribosomal-entry-site-mediated regulation, within GC B cells, and this must await improved techniques for measuring translational regulation in rare cell populations.

In summary, we observed that the regulation of gene expression in B cells by PTBP1 was necessary for GC B cell proliferation. At the cellular level, PTBP1 functioned in GC B cells to promote

the rapid progression through the late S phase of the cell cycle. At the molecular level, we identified the role of PTBP1 in regulating the quantitative and qualitative changes in the transcriptome that were part of the c-MYC-dependent gene-expression program. Post-transcriptional regulation by PTBP1 acted in concert with transcription factors such as c-MYC to integrate anabolic metabolism and cell-cycle progression and to drive the production of high-affinity antibodies.

Methods

Methods, including statements of data availability and any associated accession codes and references, are available at <https://doi.org/10.1038/s41590-017-0035-5>.

Received: 26 June 2017; Accepted: 12 December 2017;

Published online: 22 January 2018

References

- Mesin, L., Ersching, J. & Victora, G. D. Germinal center B cell dynamics. *Immunity* **45**, 471–482 (2016).
- Bannard, O. & Cyster, J. G. Germinal centers: programmed for affinity maturation and antibody diversification. *Curr. Opin. Immunol.* **45**, 21–30 (2017).
- Gitlin, A. D. et al. Humoral immunity. T cell help controls the speed of the cell cycle in germinal center B cells. *Science* **349**, 643–646 (2015).
- Gitlin, A. D., Shulman, Z. & Nussenzweig, M. C. Clonal selection in the germinal centre by regulated proliferation and hypermutation. *Nature* **509**, 637–640 (2014).
- Calado, D. P. et al. The cell-cycle regulator c-Myc is essential for the formation and maintenance of germinal centers. *Nat. Immunol.* **13**, 1092–1100 (2012).
- Dominguez-Sola, D. et al. The proto-oncogene MYC is required for selection in the germinal center and cyclic reentry. *Nat. Immunol.* **13**, 1083–1091 (2012).
- Chou, C. et al. The transcription factor AP4 mediates resolution of chronic viral infection through amplification of germinal center B cell responses. *Immunity* **45**, 570–582 (2016).
- Ersching, J. et al. Germinal Center selection and affinity maturation require dynamic regulation of mTORC1 kinase. *Immunity* **46**, 1045–1058 (2017).
- Sander, S. et al. PI3 kinase and FOXO1 transcription factor activity differentially control b cells in the germinal center light and dark zones. *Immunity* **43**, 1075–1086 (2015).
- Dominguez-Sola, D. et al. The FOXO1 transcription factor instructs the germinal center dark zone program. *Immunity* **43**, 1064–1074 (2015).
- Inoue, T. et al. The transcription factor Foxo1 controls germinal center B cell proliferation in response to T cell help. *J. Exp. Med.* **214**, 1181–1198 (2017).
- Martinez, N. M. & Lynch, K. W. Control of alternative splicing in immune responses: many regulators, many predictions, much still to learn. *Immunol. Rev.* **253**, 216–236 (2013).
- Schaub, A. & Glasmacher, E. Splicing in immune cells—mechanistic insights and emerging topics. *Int. Immunol.* **29**, 173–181 (2017).
- Diaz-Muñoz, M. D. et al. The RNA-binding protein HuR is essential for the B cell antibody response. *Nat. Immunol.* **16**, 415–425 (2015).
- Chang, X., Li, B. & Rao, A. RNA-binding protein hnRNPLL regulates mRNA splicing and stability during B-cell to plasma-cell differentiation. *Proc. Natl Acad. Sci. USA* **112**, E1888–E1897 (2015).
- Berkovits, B. D. & Mayr, C. Alternative 3' UTRs act as scaffolds to regulate membrane protein localization. *Nature* **522**, 363–367 (2015).
- Pioli, P. D., Debnath, I., Weis, J. J. & Weis, J. H. Zfp318 regulates IgD expression by abrogating transcription termination within the *Ighm/Ighd* locus. *J. Immunol.* **193**, 2546–2553 (2014).
- Keppetipola, N., Sharma, S., Li, Q. & Black, D. L. Neuronal regulation of pre-mRNA splicing by polypyrimidine tract binding proteins, PTBP1 and PTBP2. *Crit. Rev. Biochem. Mol. Biol.* **47**, 360–378 (2012).
- Sawicka, K., Bushell, M., Spriggs, K. A. & Willis, A. E. Polypyrimidine-tract-binding protein: a multifunctional RNA-binding protein. *Biochem. Soc. Trans.* **36**, 641–647 (2008).
- Gooding, C., Kemp, P. & Smith, C. W. J. A novel polypyrimidine tract-binding protein paralog expressed in smooth muscle cells. *J. Biol. Chem.* **278**, 15201–15207 (2003).
- Baralle, F. E. & Giudice, J. Alternative splicing as a regulator of development and tissue identity. *Nat. Rev. Mol. Cell Biol.* **18**, 437–451 (2017).
- Tan, L.-Y. et al. Generation of functionally distinct isoforms of PTBP3 by alternative splicing and translation initiation. *Nucleic Acids Res.* **43**, 5586–5600 (2015).
- Knoch, K.-P. et al. Polypyrimidine tract-binding protein promotes insulin secretory granule biogenesis. *Nat. Cell Biol.* **6**, 207–214 (2004).

24. Knoch, K.-P. et al. PTBP1 is required for glucose-stimulated cap-independent translation of insulin granule proteins and coxsackieviruses in beta cells. *Mol. Metab.* **3**, 518–530 (2014).
25. Vavassori, S., Shi, Y., Chen, C. C., Ron, Y. & Covey, L. R. In vivo post-transcriptional regulation of CD154 in mouse CD4⁺ T cells. *Eur. J. Immunol.* **39**, 2224–2232 (2009).
26. Porter, J. E., Vavassori, S. & Covey, L. R. A polypyrimidine tract-binding protein-dependent pathway of mRNA stability initiates with CpG activation of primary B cells. *J. Immunol.* **181**, 3336–3345 (2008).
27. Boutz, P. L. et al. A post-transcriptional regulatory switch in polypyrimidine tract-binding proteins reprograms alternative splicing in developing neurons. *Genes. Dev.* **21**, 1636–1652 (2007).
28. David, C. J., Chen, M., Assanah, M., Canoll, P. & Manley, J. L. HnRNP proteins controlled by c-Myc deregulate pyruvate kinase mRNA splicing in cancer. *Nature* **463**, 364–368 (2010).
29. Sabò, A. et al. Selective transcriptional regulation by Myc in cellular growth control and lymphomagenesis. *Nature* **511**, 488–492 (2014).
30. Suckale, J. et al. PTBP1 is required for embryonic development before gastrulation. *PLoS One* **6**, e16992 (2011).
31. Spellman, R., Llorian, M. & Smith, C. W. J. Crossregulation and functional redundancy between the splicing regulator PTB and its paralogs nPTB and ROD1. *Mol. Cell.* **27**, 420–434 (2007).
32. Vuong, J. K. et al. PTBP1 and PTBP2 serve both specific and redundant functions in neuronal pre-mRNA splicing. *Cell Rep.* **17**, 2766–2775 (2016).
33. Victora, G. D. et al. Identification of human germinal center light and dark zone cells and their relationship to human B-cell lymphomas. *Blood* **120**, 2240–2248 (2012).
34. Liberzon, A. et al. The Molecular Signatures Database (MSigDB) hallmark gene set collection. *Cell. Syst.* **1**, 417–425 (2015).
35. Zeman, M. K. & Cimprich, K. A. Causes and consequences of replication stress. *Nat. Cell. Biol.* **16**, 2–9 (2014).
36. Dayton, T. L., Jacks, T. & Vander Heiden, M. G. PKM2, cancer metabolism, and the road ahead. *EMBO Rep.* **17**, 1721–1730 (2016).
37. La Porta, J., Matus-Nicodemus, R., Valentín-Acevedo, A. & Covey, L. R. The RNA-binding protein, polypyrimidine tract-binding protein 1 (PTBP1) is a key regulator of CD4 T cell activation. *PLoS One* **11**, e0158708 (2016).
38. Shibayama, M. et al. Polypyrimidine tract-binding protein is essential for early mouse development and embryonic stem cell proliferation. *FEBS J.* **276**, 6658–6668 (2009).
39. Boothby, M. & Rickert, R. C. Metabolic regulation of the immune humoral response. *Immunity* **46**, 743–755 (2017).
40. Chan, L. N. et al. Metabolic gatekeeper function of B-lymphoid transcription factors. *Nature* **542**, 479–483 (2017).
41. Suzuki, K., Kumanogoh, A. & Kikutani, H. Semaphorins and their receptors in immune cell interactions. *Nat. Immunol.* **9**, 17–23 (2008).
42. Jung, C.-R. et al. Enigma negatively regulates p53 through MDM2 and promotes tumor cell survival in mice. *J. Clin. Invest.* **120**, 4493–4506 (2010).
43. Dufort, F. J. et al. Glucose-dependent de novo lipogenesis in B lymphocytes: a requirement for ATP-citrate lyase in lipopolysaccharide-induced differentiation. *J. Biol. Chem.* **289**, 7011–7024 (2014).
44. Hann, S. R. MYC cofactors: molecular switches controlling diverse biological outcomes. *Cold Spring Harb. Perspect. Med.* **4**, a014399 (2014).
45. Cortés, M. & Georgopoulos, K. Aiolos is required for the generation of high affinity bone marrow plasma cells responsible for long-term immunity. *J. Exp. Med.* **199**, 209–219 (2004).
46. Quéméneur, L. et al. Differential control of cell cycle, proliferation, and survival of primary T lymphocytes by purine and pyrimidine nucleotides. *J. Immunol.* **170**, 4986–4995 (2003).
47. Ke, Y., Ash, J. & Johnson, L. F. Splicing signals are required for S-phase regulation of the mouse thymidylate synthase gene. *Mol. Cell. Biol.* **16**, 376–383 (1996).
48. Nowak, U., Matthews, A. J., Zheng, S. & Chaudhuri, J. The splicing regulator PTBP2 interacts with the cytidine deaminase AID and promotes binding of AID to switch-region DNA. *Nat. Immunol.* **12**, 160–166 (2011).
49. Hogenbirk, M. A. et al. Differential programming of B cells in AID deficient mice. *PLoS One* **8**, e69815 (2013).

Acknowledgements

We thank D. L. Black (Brain Research Institute, University of California) for *Ptbp2^{tm1}* mice; M. Reth (Max Planck Institute of Immunobiology and Epigenetics) for *Cd79a^{Cre}* mice; M. Busslinger (Research Institute of Molecular Pathology) for *Aicda^{Tg-Cre}* mice; B. P. Sleckman (Weill Cornell Medicine Pathology & Laboratory Medicine) for *Myc^{GFP/GFP}* mice; F. W. Alt (Department of Genetics, Harvard Medical School) for *Rag2^{-/-}* mice; J. Ule, N. Haberman and T. Curk for help with iCLIP data; G. Butcher for assistance in generating monoclonal antibodies to PTBP3; K. Bates, D. Sanger, A. Davis, the Biological Support Unit, Flow Cytometry and Bioinformatics Facilities for technical assistance; and M. Spivakov and members of the Turner and Smith laboratories for helpful discussions. Supported by The Biotechnology and Biological Sciences Research Council (BB/J004472/1 and BB/J00152X/1 to M.T.), the Wellcome Trust (200823/Z/16/Z to M.T.) and Bloodwise (14022 to M.T.).

Author contributions

E.M.-C., C.W.J.S. and M.T. designed experiments; E.M.-C., M. Screen, M.D.D.-M., S.E.B. and G.L. performed experiments and analyzed data; E.M.-C. carried out computational analyses; R.M.R.C. ran DaPars; M. Solimena provided *Ptbp1^{tm1Mbol}* mice and antibody to PTBP2; and E.M.-C. and M.T. wrote the manuscript with input from the co-authors.

Competing interests

The authors declare no competing financial interests.

Additional information

Supplementary information is available for this paper at <https://doi.org/10.1038/s41590-017-0035-5>.

Reprints and permissions information is available at www.nature.com/reprints.

Correspondence and requests for materials should be addressed to M.T.

Publisher's note: Springer Nature remains neutral with regard to jurisdictional claims in published maps and institutional affiliations.

Methods

Mice. All mice were on a C57BL/6 background. For bone marrow chimera experiments, B6.SJL were used as recipients. Conditional-knockout mice used in this study derive from crossing the following transgenic strains: *Ptbp1^{fl/fl}* (*Ptbp1^{tm1(Ms6)}*)³⁰, *Ptbp2^{fl/fl}* (*Ptbp2^{tm1.1Dblk}*)⁵⁰, *Cd79a^{Cre}* (*Cd79a^{tm1(Cre)Reth}*)⁵¹ and *Aicda*Tg-Cre (Tg(*Aicda-Cre*)^{9^{Mbu})⁵² as specified in the Results section. GFP-c-MYC (*Myctm1Slck*) reporter mice⁵³ and *Rag2^{-/-}* mice (*Rag2^{tm1Fwa}*)⁵⁴ were also used in this study.}

Rats. RT7b rats were used for the generation of monoclonal antibodies to PTBP3.

Immunization protocols and in vivo BrdU administration. All procedures performed were approved by the Babraham Institute's Animal Welfare and Experimentation Committee and the UK Home Office and are in compliance with all relevant ethical regulations. Mice immunized with alum-NP-KLH received 100 µg NP-KLH (Biosearch Technologies) intraperitoneally. Mice immunized with SRBCs received 2 × 10⁸ SRBCs intraperitoneally. For in vivo BrdU incorporation experiments, mice received 2 mg BrdU intraperitoneally 1.5 h before they were culled. Bone marrow competitive chimeras were generated by reconstitution of lethally irradiated (500 rads, twice) B6.SJL mice with 3 × 10⁶ bone marrow cells derived from B6.SJL mice at a 1:1 ratio with *CD79a^{Cre/+}Ptbp1^{fl/fl}* (cKO) or *CD79a^{+/+}Ptbp1^{fl/fl}* control bone marrow cells, administered intravenously. *Rag2^{-/-}* bone marrow chimeras were generated by reconstitution of sublethally irradiated (500 rads, once) *Rag2^{-/-}* mice with 3 × 10⁶ bone marrow cells from *Cd79a^{+/+}Ptbp1^{fl/fl}Myc^{GFP/GFP}* or *Cd79a^{Cre/+}Ptbp1^{fl/fl}Myc^{GFP/GFP}* mice, administered intravenously. Mice used in immunization experiments with different genotypes were sex and age matched. Whenever possible, littermates of the same sex but different genotypes were kept in the same cages to avoid confounding effects. Male and female mice were used in this study. Except in bone marrow-reconstitution experiments, immunizations were carried out on 8- to 14-week-old mice. Bone marrow competitive chimeras were immunized 15 weeks after reconstitution. *Rag2^{-/-}* bone marrow chimeras were immunized 13 weeks after reconstitution.

Flow cytometry. Single-cell suspensions were prepared from tissues by passing the tissues through cell strainers with 70 and 40 µm pore sizes. After Fc receptors (CD16/32) were blocked with the monoclonal rat antibody 2.4G2 (BioXcell), cells were stained with antibodies (Supplementary Table 6) in 1% FCS PBS at 4°C. Cell viability was assessed by staining cells with the Fixable Viability Dye eFluor 780 dye from eBioscience. Unless otherwise stated, dead cells were always excluded from the analysis. For intracellular staining cells were fixed and permeabilized with the BD Cytofix/Cytoperm Fixation and Permeabilization Solution from BD Biosciences. Nuclear permeabilization was carried out with the Permeabilization Buffer Plus from BD Biosciences when cells were prepared from the spleen or by freezing fixed cells in FCS containing 10% DMSO at -80°C when cells were isolated from the bone marrow. Intracellular staining was carried out by incubating permeabilized cells with combinations of antibodies (Supplementary Table 6) diluted in BD Perm/Wash Buffer. For some intracellular staining, such as for the detection of PTBP1, the incubation with antibodies was carried out for 4 h at room temperature. A Foxp3/Transcription Factor Staining Buffer Set from eBioscience was also occasionally used. Staining of BrdU and DNA was carried out using the FITC BrdU Flow Kit from BD Biosciences. Monoclonal antibodies to PTBP1, PTBP2 and PTBP3 were directly conjugated using Alexa Fluor 488, Alexa Fluor 647 or Pacific Blue Antibody Labeling Kits from ThermoFisher Scientific.

Detection of NP specific immunoglobulins. NP-specific antibodies of different affinities were detected as previously described⁴⁴ using two different conjugation ratios of NP to BSA. Detection of NP-specific antibodies with low and high affinity was done by coating ELISA plates with a ratio of at least 20 NP moieties per BSA molecule (NP20, Biosearch Technologies). Detection of NP-specific antibodies with only high affinity was performed by coating ELISA plates with a ratio of 2 NP moieties per BSA molecule. Endpoint titers were calculated from serial dilutions of serum samples.

Isolation of B cells and ex vivo stimulation. B cells were isolated from spleens of mice after preparing a single-cell suspension by MACS negative depletion with a B cell isolation kit (Cat. # 130-090-862 from Miltenyi). When stimulated ex vivo, B cells were cultured in IMDM (Cat. # 21980, ThermoFisher Scientific) with L-glutamine and 25 mM HEPES, supplemented with 10% heat-inactivated FCS, 50 µM β-mercaptoethanol, penicillin and streptomycin (GIBCO). Cells were stimulated with LPS (10 µg/ml 127:B0, Sigma); anti-CD40 (FGK4.2, 10 µg/ml, from BioXcell), IL-4 (10 ng/ml) and IL-5 (10 ng/ml) or anti-IgM (B7.6, 9 µg/ml, from Jackson ImmunoResearch) and IL-4 (10 ng/ml). In proliferation assays, B cells were labeled with CellTrace Violet (ThermoFisher) before culture. 1.5 × 10⁵ B cells were added per well in 96-well plates. Cells were counted using counting beads analyzed by flow cytometry. In PKM stimulation experiments DASA-58⁵⁵ (MedChem Express, Cat. # HY-19330-1ml) was added to the cultures. The same

amount of DMSO as the highest concentration of DASA-58 was added to the cultures as vehicle control.

PTBP1 iCLIP. iCLIP reveals the site of direct binding of a RBP to RNA at single-nucleotide resolution. This is achieved first by the covalent binding of the RBP to its cognate RNA in intact cells by UV irradiation and second, through the truncation of cDNA synthesis when reverse polymerase encounters residual peptides derived from the RBP at the site of cross-linking to the RNA⁵⁶. PTBP1 immunoprecipitation was carried out with monoclonal antibody CLONE 1 (ThermoFisher Scientific, Cat. # 32-4800) coupled to protein A/G magnetic beads (Pierce, Cat. #88802) and UV-cross-linked (150mJ/cm²) cell extracts of primary B cells stimulated ex vivo for 48 h with LPS as described above. B cells were isolated from several C57BL/6 female mice and were pooled together before stimulation. 30 × 10⁶ cells were used in each immunoprecipitation and were lysed in 50 mM Tris-HCl, pH7.4, 100 mM NaCl, 1% NP-40 and 0.1% SDS lysis buffer. Before immunoprecipitation of PTBP1, cell extracts were treated with Turbo DNase (Ambion, #AM2239) and small amounts of RNase I (1.5 to 3 units) from Ambion (Cat. # AM2294). Immunoprecipitates were separated by SDS-PAGE and RNA-protein complexes were transferred to a nitrocellulose membrane. Protein-RNA complexes were isolated from the nitrocellulose membrane after cutting only the areas (from ~75 to ~120 kDa) where PTBP1 was expected to be cross-linked to long RNAs. After protein digestion, RNA was isolated and cDNA was synthesized by reverse transcription. At this time bar-coded primers were used that allow the identification of cDNAs generated from the same RNA molecule (with a random unknown four-nucleotide barcode), which allows the discrimination of PCR duplicates, and then multiplexing of several samples together. Amplification of iCLIP cDNA libraries was done with 20–27 PCR cycles. We carried out five replicates. Multiplexed iCLIP cDNA libraries were sequenced on an Illumina HiSeq 2000 platform on a 50-bp single-ended mode. Negative controls (immunoprecipitation of PTBP1 from non-UV-cross-linked lysates and immunoprecipitation with a mouse IgG1 negative isotype-matched control antibody(MOPC-1, Sigma, Cat. # 015K4806) resulted in very little isolated RNA, from which no cDNA library could be generated.

Computational processing of iCLIP data. Identification of transcriptome-wide PTBP1 binding sites was done as previously described⁵⁶. In brief, mapping of cDNAs to the mouse genome (mm10) was carried out with Bowtie, and those reads that mapped to the same location and had the same random four-nucleotide barcode were considered PCR duplicates and collapsed as a single cDNA molecule. A PTBP1-binding site (or X-link site) is the nucleotide before the first nucleotide of a mapped cDNA molecule. An FDR value, which determines the probability of a X-link site to appear by chance, was calculated (as described⁵⁶) for each X-link site. iCLIP is highly dependent on RNA abundance and therefore, is not an absolute measurement of RNA-protein interactions. For this reason we pooled the five replicates together before calculating FDRs for each X-link site.

Generation of mRNAseq libraries. LZ and DZ GC B cells were sorted by flow cytometry from *CD79a^{Cre/+}Ptbp1^{fl/fl}* or *CD79a^{+/+}Ptbp1^{fl/fl}* mice immunized with alum-NP-KLH 7 d before. Single-cell suspensions were prepared from spleens of immunized mice. Erythrocytes were lysed and GC B cells were enriched before sorting by flow cytometry by depletion of cells stained with biotinylated anti-IgD (11-26c.2a, Southern Biotech), anti-CD3e (145-2C11, eBioscience), anti-Gr1 (RB6-8C5, ThermoFisher) and anti-Ter119 (TER-119, eBioscience) by MACS. Four biological replicates were used per condition. In each biological replicate, GC B cell-enriched splenocytes from three to five mice of the same genotype and sex were pooled together before sorting by flow cytometry. LZ and DZ GC B cells were sorted from the same GC B cell-enriched samples. LZ and DZ GC B cells from *CD79a^{+/+}Ptbp1^{fl/fl}* and *CD79a^{Cre/+}Ptbp1^{fl/fl}* mice were sorted on the same day. Two biological replicates per condition were from female mice and two from male mice.

RNA was prepared using the RNeasy Micro Kit kit from Qiagen (Cat. #74004) from ~25,000 cells to ~200,000 cells. RNA quality was analyzed on a 2100 Bioanalyzer (Agilent). RNA integrity numbers ranged from 9.1 ng to 10.2 ng of total RNA was used to generate cDNA from polyadenylated transcripts using the SMART-Seq v4 Ultra low input RNA kit from Clontech (Cat. #634888). cDNA quality was analyzed on a 2100 Bioanalyzer (Agilent). 0.5 ng cDNA were used to prepare the mRNAseq libraries with eight cycles of PCR using the Ultra Low library preparation kit v2 from Clontech (Cat. #634899). Compatible barcoded libraries were multiplexed and sequenced across three lanes on an Illumina HiSeq 2500 platform on a 100-bp paired-end mode.

Analysis of mRNAseq libraries generated in this study. Trimming of libraries was carried out with TrimGalore (v0.4.2) using default parameters. After that, reads were mapped to the mouse *Mus_musculus.GRCm38* genome with Hisat2⁵⁷ using -p 7 -t -phred33-quals-no-mixed-no-discordant parameters and providing a known splice sites file generated from the *Mus_musculus.GRCm38.70.gtf* annotation. Counting of reads mapping to all exons of a particular gene was done with HTSeq⁵⁸ using the *Mus_musculus.GRCm38.84.gtf* annotation and default parameters. DESeq2 (v1.12.1)⁵⁹ was used to calculate differential RNA abundance between two conditions at the whole gene level by quantifying differences in RNA

complementary to all annotated exons of a particular gene in the RNAseq data. Information on the genotype and sex of the animals was included in the design formula in order to control for variation in the data due to the sex differences in the samples. DESeq2 results were only considered for genes that are expressed with at least 1 FPKM in any of the conditions. Significant differentially abundant genes are those that have an adjusted P value of < 0.1 .

Differential AS was analyzed with rMATS (v3.2.2)⁶⁰. rMATS uses an exon-centric approach to discover both annotated and unannotated AS events in a reference transcriptome. To compare changes in AS between two conditions, rMATS calculates first inclusion levels (defined as the proportion of transcripts containing that particular AS segment) for five different types of AS events: skipped exons (SE), mutually exclusive exons (MXE), alternative 5' splice sites (A5SSs) alternative 3' splice sites (A3SSs) and retained introns in each of the two conditions (Supplementary Fig. 4e). Subsequently, rMATS calculates inclusion level differences by subtracting the inclusion levels of condition one from the inclusion levels of condition two (Supplementary Fig. 4f). The version of rMATS used accepts only mapped reads of a particular length. For this reason, libraries trimmed with Trimgalore as described above were further trimmed with Trimmomatic v0.35⁶¹ so that all reads had a length of 98 bp. Reads shorter than 98 bp were discarded. These reads of only 98 bp were then mapped to the mouse genome using Hisat2 as described above. rMATS was run on a paired mode (-analysis P) to analyze differential AS between two conditions using the *Mus_musculus.GRCm38.84.gtf* annotation. Only results obtained with reads that map to exon-exon junctions were used for further analysis. Genes that have less than 1 FPKM in the analyzed conditions were discarded. Significantly differentially spliced events are those that have an FDR < 0.05 . A cut-off of an inclusion-level difference greater than 10% (0.1) was introduced for significant differentially alternatively spliced events.

We assigned PTBP1 binding to the vicinity of a differentially alternatively spliced event if we found at least a significant PTBP1-binding site in our iCLIP data in the following cases. Skipped exons (SE) were considered to be bound by PTBP1 if a binding site was identified on the SE, on the intronic 500 nucleotides upstream and downstream of the SE. 3' splice site (SS) and 5' SS, respectively; on the upstream flanking constitutive exon and the intronic 500 nucleotides downstream of its 5' SS or on the downstream flanking constitutive exon and the intronic 500 nucleotides upstream of its 3' SS. Mutually exclusive exons (MXEs) were bound by PTBP1 if a binding site was found on any of the MXE and the intronic 500 nucleotides upstream and downstream of their 3' SS and 5' SS, respectively; on the upstream flanking constitutive and the intronic 500 nucleotides downstream of its 5' SS or on the downstream flanking constitutive exon and the intronic 500 nucleotides upstream of its 3' SS. Alternative 5' splice sites (A5SSs) were bound by PTBP1 if a binding site was found on the longer exon generated by the A5SS, the intronic 500 nucleotides downstream of the 5SS of the longest A5SS exon or on the flanking constitutive exon downstream of the A5SS and the intronic 500 nucleotides upstream of its 3SS. Alternative 3' splice sites (A3SSs) were bound by PTBP1 if a binding site was found on the longer exon generated by the A3SS, the intronic 500 nucleotides upstream of the 3SS of the longest A3SS exon or on the flanking constitutive exon upstream of the A3SS and the intronic 500 nucleotides downstream of its 5SS. A retained intron was bound by PTBP1 if a binding site was found on the exon resulting from intron retention.

Differential alternative polyadenylation site usage. Alternative polyadenylation (APA) usage was assessed with the 'Dynamic analysis of Alternative PolyAdenylation from RNA-Seq' algorithm (DaPars v0.9.1⁶²). DaPars computes first the percentage of distal polyadenylation (poly(A)) site usage index (PDUI) and, subsequently, computes changes in PDUI between two conditions (Δ PDUI). Annotated gene models were generated from mouse genome build GRCm38/mm10, facilitating the prediction of proximal de novo APA sites as well as long and short 3' UTR expression levels. Bedtools v2.25.0 was used to convert the RNA-seq BAM files to BedGraph format, and these files were then used as input for DaPars to identify dynamic APA usage between the control and knockout mice. Differences in APA were considered for those genes with an absolute change in percentage of distal polyA site usage of $> 20\%$ (Δ PDUI $> |0.2|$), an adjusted P value of < 0.05 and a fitted value of the regression model used to identify the proximal poly(A) site > 500 .

Analysis of mRNAseq libraries previously published. Published RNAseq data⁴⁹ were trimmed with Trimgalore (v0.3.8) using default parameters. Trimmed reads were mapped to the mouse genome using Tophat2 (v2.0.12)⁶³ with -p 6 -g 2 parameters and the *Mus_musculus.GRCm38.70.gtf* annotation. Mapped reads to exons of a particular gene were counted with HTSeq⁶⁴ using the *Mus_musculus.GRCm38.73.gtf* annotation and default parameters. Differential RNA abundance was calculated with DESeq2 (v1.4.5).

Published RNAseq data³ were trimmed with Trimgalore (v0.4.1). Trimmed reads were mapped to the mouse genome with Tophat2 (v2.0.12)⁶³ with -p 6 -g 2 parameters and the *Mus_musculus.GRCm38.70.gtf* annotation. Mapped reads were counted with HTSeq using the *Mus_musculus.GRCm38.75.gtf* annotation and default parameters. DESeq2 (v1.8.1) was used to analyze differential RNA abundance between GC B cells that received high levels of T cell help

(Anti-DEC-OVA) and GC B cells that did not receive high levels of T cell help (Anti-DEC-Ctrl). Genes with an adjusted P value of < 0.05 were considered to have significant differential RNA abundance. Genes with a positive change in expression (Anti-DEC-OVA vs Anti-DEC-Ctrl; \log_2 values) were chosen as genes with higher expression in GC B cells receiving high levels of T cell help than in GC B cells that are not receiving high levels of T cell help (used in Fig. 5).

Published RNAseq data⁷ were trimmed with Trimgalore (v0.4.2_dev). Trimmed reads were mapped to the mouse genome using Hisat2 (v2.0.5)⁵⁷ and the *Mus_musculus.GRCm38* genome. Reads mapping to all exons of a particular gene were counted with HTSeq using the *Mus_musculus.GRCm38.84.gtf* annotation and default parameters. Differential RNA abundance between two conditions was calculated with DESeq2 v1.12.4. Genes with an increased RNA abundance in AP4⁺ Myc⁺ LZ GC B cells compared to AP4⁺ Myc⁻ LZ GC B cells used in Fig. 5 were defined as genes with an adjusted P value of < 0.05 whose change in expression (AP4⁺ Myc⁺ LZ GC B cells versus AP4⁺ Myc⁻ LZ GC B cells; \log_2 values) was equal or greater than 1.5.

Calculation of FPKM. FPKM values (fragments per kilobase of exon per million reads mapped) were used to compare expression values of different genes or transcripts and to filter genes based on their expression level. FPKM values were calculated with the Cuffnorm option of Cufflinks (v2.2.1)⁶⁴ using the geometric normalization method and the mapped reads of the different RNAseq libraries described above. The following annotations were used to calculate FPKM values from the different studies: *Mus_musculus.GRCm38.84.gtf* was used with our RNAseq data and published data⁷, *Mus_musculus.GRCm38.83.gtf* was used with published data⁴⁹ and *Mus_musculus.GRCm38.75.gtf* was used with published data³.

GO analysis. Gene ontology (GO) term-enrichment analysis was carried out with GOrilla⁶⁵. A background list of genes (genes expressed with at least 1 FPKM in the conditions analyzed) was included in the analysis. For visualization purposes, when several related terms were significantly enriched, the term with a higher percentage of significant genes with different mRNA abundance or AS was chosen to be presented in Supplementary Fig. 5.

RNAseq data visualization. Sashimi plots, which show RNAseq coverage and reads mapping across exon-exon junctions, were generated using the IGV genome browser.

Analysis of *Jh4* mutations. Mutations in the *Jh4* intronic region were analyzed as previously described⁴. In brief, genomic DNA was isolated from GC B cells sorted by flow cytometry from the spleen of mice immunized with alum-NP-KLH 7 d before. GC B cells from two to four mice of the same genotype and sex were pooled together. *Jh4* intronic regions were amplified with the primers Jh4-intron Forward and Jh4-intron Reverse in using the PfuUltra II Fusion HS DNA Polymerase (Agilent Technologies) in PCR with 35 cycles, 57 °C annealing temperature and 15 s extension time at 72 °C. PCR amplified *Jh4* intronic regions were cloned using the Zero Blunt TOPO PCR Cloning Kit (ThermoFischer scientific). Mutation frequencies were calculated by dividing the total number of mutations identified in each replicate by the total length of amplified DNA (565 bp per clone analyzed, which is the genomic region amplified by PCR without taking into account the regions complementary to the primers).

Generation of monoclonal antibody to PTBP3. RT7b rats were immunized with a GST-PTBP3 fusion protein containing amino acids 279–359 of the full-length mouse PTBP3 generated in *Escherichia coli*. After several immunizations, spleens were isolated and fused to the IR983F rat myeloma cell line. Hybridomas were screened by immunoblot using HEK2 cell lysates expressing mouse PTBP3, PTBP1 or PTBP2-GFP fusion proteins. Two hybridomas secreted IgG2a antibodies specific for PTBP3: MAC454 and MAC455. Monoclonal antibodies secreted by these two hybridomas were purified by affinity chromatography using protein G.

Immunoblot analysis. In order to analyze PKM1 and PKM2 expression, 12 μ g of proteins extracted from B cells isolated as described above from individual mice and stimulated or not with LPS for 48 h were separated by 10% SDS-PAGE and transferred to a nitrocellulose membrane. PKM1 detection was carried out with a rabbit monoclonal antibody (clone D30G6, Cell Signaling) and PKM2 was detected with a rabbit monoclonal antibody (clone D78A4, Cell signaling). Visualization of anti-PKM1 and anti-PKM2 was carried out with an HRP-conjugated goat anti-rabbit (Cat # 2020-10, Dako). Immunoblot analysis of the different PTBPs was carried out with 15 μ g of proteins extracted from B cells isolated as described above from individual mice separated by 10% SDS-PAGE and transferred to a nitrocellulose membrane. Mouse monoclonal primary antibodies were detected with TrueBlot HRP-conjugated anti-mouse (eBioscience, Cat. #18-8817-31). Rat monoclonal primary antibodies were detected with HRP-conjugated goat anti-rat (Cat. #P0450, Dako). Rabbit primary antibodies were detected with HRP-conjugated goat anti-rabbit (Cat. #2020-10, Dako).

Quantification and statistical analysis. Flow-cytometry data were analyzed using FlowJo (versions 10.0.8r1 or 9.8.3). Analysis and quantification of RNAseq

and iCLIP experiments is detailed in the following sections of methods: Analysis of mRNAseq libraries generated in this study, Analysis of mRNAseq libraries previously published, Calculation of FPKM and Computational processing of iCLIP data. Statistical significance of flow cytometry data was assessed using Prism (versions 7 or 6). The details of the tests used in different experiments can be found in the figure legends.

Life Sciences Reporting Summary. Further information on experimental design and reagents is available in the Life Sciences Reporting Summary.

Data availability. mRNAseq and iCLIP data that support the findings of this study have been deposited in GEO with the accession code [GSE100969](https://www.ncbi.nlm.nih.gov/geo/query/acc.cgi?acc=GSE100969).

References

- Li, Q. et al. The splicing regulator PTBP2 controls a program of embryonic splicing required for neuronal maturation. *eLife* **3**, e01201 (2014).
- Hobeika, E. et al. Testing gene function early in the B cell lineage in mb1-cre mice. *Proc. Natl Acad. Sci. USA* **103**, 13789–13794 (2006).
- Kwon, K. et al. Instructive role of the transcription factor E2A in early B lymphopoiesis and germinal center B cell development. *Immunity* **28**, 751–762 (2008).
- Huang, C.-Y., Bredemeyer, A. L., Walker, L. M., Bassing, C. H. & Sleckman, B. P. Dynamic regulation of c-Myc proto-oncogene expression during lymphocyte development revealed by a GFP-c-Myc knock-in mouse. *Eur. J. Immunol.* **38**, 342–349 (2008).
- Shinkai, Y. et al. RAG-2-deficient mice lack mature lymphocytes owing to inability to initiate V(D)J rearrangement. *Cell* **68**, 855–867 (1992).
- Anastasiou, D. et al. Pyruvate kinase M2 activators promote tetramer formation and suppress tumorigenesis. *Nat. Chem. Biol.* **8**, 839–847 (2012).
- König, J. et al. iCLIP reveals the function of hnRNP particles in splicing at individual nucleotide resolution. *Nat. Struct. Mol. Biol.* **17**, 909–915 (2010).
- Kim, D., Langmead, B. & Salzberg, S. L. HISAT: a fast spliced aligner with low memory requirements. *Nat. Methods* **12**, 357–360 (2015).
- Anders, S., Pyl, P. T. & Huber, W. HTSeq—a Python framework to work with high-throughput sequencing data. *Bioinformatics* **31**, 166–169 (2015).
- Love, M. I., Huber, W. & Anders, S. Moderated estimation of fold change and dispersion for RNA-seq data with DESeq2. *Genome Biol.* **15**, 550 (2014).
- Shen, S. et al. rMATS: robust and flexible detection of differential alternative splicing from replicate RNA-Seq data. *Proc. Natl Acad. Sci. USA* **111**, E5593–E5601 (2014).
- Bolger, A. M., Lohse, M. & Usadel, B. Trimmomatic: a flexible trimmer for Illumina sequence data. *Bioinformatics* **30**, 2114–2120 (2014).
- Xia, Z. et al. Dynamic analyses of alternative polyadenylation from RNA-seq reveal a 3′-UTR landscape across seven tumour types. *Nat. Commun.* **5**, 5274 (2014).
- Kim, D. et al. TopHat2: accurate alignment of transcriptomes in the presence of insertions, deletions and gene fusions. *Genome Biol.* **14**, R36 (2013).
- Trapnell, C. et al. Differential gene and transcript expression analysis of RNA-seq experiments with TopHat and Cufflinks. *Nat. Protoc.* **7**, 562–578 (2012).
- Eden, E., Navon, R., Steinfeld, I., Lipson, D. & Yakhini, Z. GOrilla: a tool for discovery and visualization of enriched GO terms in ranked gene lists. *BMC Bioinforma.* **10**, 48 (2009).

Life Sciences Reporting Summary

Nature Research wishes to improve the reproducibility of the work that we publish. This form is intended for publication with all accepted life science papers and provides structure for consistency and transparency in reporting. Every life science submission will use this form; some list items might not apply to an individual manuscript, but all fields must be completed for clarity.

For further information on the points included in this form, see [Reporting Life Sciences Research](#). For further information on Nature Research policies, including our [data availability policy](#), see [Authors & Referees](#) and the [Editorial Policy Checklist](#).

▶ Experimental design

1. Sample size

Describe how sample size was determined.

A priori the effect size and standard deviation of our tested groups are unknown, thus no specific sample sizes were calculated. In exploratory experiments a sample size of 3 to 6 animals per group was used. This was sufficient to detect relevant differences.

2. Data exclusions

Describe any data exclusions.

In Figure 1b, data from one mouse was excluded because the fluorescence intensity for the PTBP3 intracellular staining was 1.5-fold higher than the mean for both non-GC and GC B cells. The reason why this data point was excluded is because this was seen only once in one out three experiments. In the experiment shown in Figure 3 one mouse had a expansion of non lymphoid cells. Data collected from this mouse was excluded. In Supplementary Figure 3c data from two mice were excluded from the graphs showing absolute numbers because they had splenomegaly. Rarely, the fluorescence intensity of the BrdU staining in GC B cells was not sufficient to allow proper gating of cells in early/late S-phase. Data from mice where this occurred were excluded from the analysis. Occasionally control or conditional KO mice did not respond at all to the immunisation protocols. The data from these mice is not included in the figures.

3. Replication

Describe whether the experimental findings were reliably reproduced.

All replication experiments were successful.

4. Randomization

Describe how samples/organisms/participants were allocated into experimental groups.

For experiments with mice, samples were randomly analyzed with out separating mice by genotype. For mRNAseq experiments, four biological replicates were used per condition. In each biological replicate, GC B cell-enriched splenocytes from 3 to 5 animals of the same genotype and sex were pooled together before FACS sorting. LZ and DZ GC B cells were sorted from the same GC B cell enriched samples. LZ and DZ GC B cells from control CD79a+Ptbp1fl/fl and CD79acre+Ptbp1fl/fl cKO mice were sorted on the same day. Two biological replicates per condition were from females and two from males.

5. Blinding

Describe whether the investigators were blinded to group allocation during data collection and/or analysis.

Blinding was used in immunizations of mice. Blinding was not used when data were collected and analyzed from the test and control groups to ensure alternate measurements for control and test samples.

Note: all studies involving animals and/or human research participants must disclose whether blinding and randomization were used.

6. Statistical parameters

For all figures and tables that use statistical methods, confirm that the following items are present in relevant figure legends (or in the Methods section if additional space is needed).

- | | |
|-------------------------------------|--|
| n/a | Confirmed |
| <input type="checkbox"/> | <input checked="" type="checkbox"/> The <u>exact sample size</u> (n) for each experimental group/condition, given as a discrete number and unit of measurement (animals, litters, cultures, etc.) |
| <input type="checkbox"/> | <input checked="" type="checkbox"/> A description of how samples were collected, noting whether measurements were taken from distinct samples or whether the same sample was measured repeatedly |
| <input type="checkbox"/> | <input checked="" type="checkbox"/> A statement indicating how many times each experiment was replicated |
| <input type="checkbox"/> | <input checked="" type="checkbox"/> The statistical test(s) used and whether they are one- or two-sided (note: only common tests should be described solely by name; more complex techniques should be described in the Methods section) |
| <input type="checkbox"/> | <input checked="" type="checkbox"/> A description of any assumptions or corrections, such as an adjustment for multiple comparisons |
| <input type="checkbox"/> | <input checked="" type="checkbox"/> The test results (e.g. P values) given as exact values whenever possible and with confidence intervals noted |
| <input checked="" type="checkbox"/> | <input type="checkbox"/> A clear description of statistics including <u>central tendency</u> (e.g. median, mean) and <u>variation</u> (e.g. standard deviation, interquartile range) |
| <input type="checkbox"/> | <input checked="" type="checkbox"/> Clearly defined error bars |

See the web collection on [statistics for biologists](#) for further resources and guidance.

► Software

Policy information about [availability of computer code](#)

7. Software

Describe the software used to analyze the data in this study.

To analyze mRNAseq libraries the following software was used: Trimgalore (v0.4.2), Hisat2 (v2.0.5), HTSeq, DESeq2 (v1.12.1, v1.4.5, v1.8.1), rMATS (v3.2.2), Trimmomatic (v0.35), R, DaPars (v0.9.1), Tophat2(v2.0.12) and Cuffnorm option of Cufflinks (v2.2.1), GOrilla, IGV genome browser.
Flow cytometry data were analyzed with FlowJo (versions 10.0.8r1 or 9.8.3).
Statistical analysis was carried out with Prism (versions 7 or 6), except for genome wide data which was carried out with the software listed above.

For manuscripts utilizing custom algorithms or software that are central to the paper but not yet described in the published literature, software must be made available to editors and reviewers upon request. We strongly encourage code deposition in a community repository (e.g. GitHub). [Nature Methods guidance for providing algorithms and software for publication](#) provides further information on this topic.

► Materials and reagents

Policy information about [availability of materials](#)

8. Materials availability

Indicate whether there are restrictions on availability of unique materials or if these materials are only available for distribution by a for-profit company.

Mouse strains are subject to MTAs as follows: Ptpb1tm1Msol Michele Solimena TU Dresden, Germany; Ptpb2tm1.1Dbk Douglas L. Black, UCLA MIMG, Los Angeles, USA; Cd79atm1(cre)Reth allele Michael Reth University of Freiburg, Germany; AicdaTg-cre (Tg(Aicda-cre)9Mbu Meinrad Busslinger, IMP Vienna, Austria; and Myctm1Slek, B.P Sleckman, Washington University, St Louis, USA.

9. Antibodies

Describe the antibodies used and how they were validated for use in the system under study (i.e. assay and species).

Novel anti-PTBP3 monoclonal antibodies are reported in this study and their validation by immunoblot of proteins derived from mouse primary B cells is shown in Supplementary Figure 2a.

Other antibodies also listed in Supplementary Table 6 used were:

PTBP1 (mouse IgG1, CLONE 1) ThermoFisher Scientific 32-4800

PTBP2 (mouse IgG2a, S43) Solimena Laboratory

PTBP3 (rat IgG2a, MAC454) Turner Laboratory

B220 (RA3-6B3) BUV395 BD Biosciences 563793

B220 (RA3-6B3) biotin eBioscience 13-0452-82

B220 (RA3-6B3) PE-Cy7 eBioscience 25-0452-82

B220 (RA3-6B2) FITC TONBO biosciences 35-0452

CD19 (6D5) FITC BioLegend 152404

CD19 (R6D5) BV785 BioLegend 115543

CD19 (1D3) BUV737 BD Biosciences 564296

CD19 (6D5) BV421 BioLegend 115538

CD95 (Jo2) BV510 BD Biosciences 563646

CD95 (Jo2) BV786 BD Biosciences 740906

CD86 (GL-1) BV421 BioLegend 105031

CD86 (GL-1) biotin BD Biosciences 553690

CD38 (90) PerCPCy5.5 BioLegend 102722

10. Eukaryotic cell lines

- State the source of each eukaryotic cell line used.
- Describe the method of cell line authentication used.
- Report whether the cell lines were tested for mycoplasma contamination.
- If any of the cell lines used are listed in the database of commonly misidentified cell lines maintained by [ICLAC](#), provide a scientific rationale for their use.

No eukaryotic cell lines were used.

No eukaryotic cell lines were used.

No eukaryotic cell lines were used.

No commonly misidentified cell lines were used.

► Animals and human research participants

Policy information about [studies involving animals](#); when reporting animal research, follow the [ARRIVE guidelines](#)

11. Description of research animals

Provide details on animals and/or animal-derived materials used in the study.

All mice used in this study were on a C57BL/6 background. For bone marrow chimera experiments, B6.SJL were used as recipients. Conditional knockout mice used in this study derive from crossing the following transgenic strains: Ptbp1fl/fl (Ptbp1tm1Msol)30, Ptbp2fl/fl (Ptbp2tm1.1Dbk)49, Cd79acre(Cd79atm1(cre)Reth)50 and AicdaTg-cre (Tg(Aicda-cre)9Mbu)51 as specified in the results section. GFP-c-MYC reporter mice Myctm1Slek 52 and Rag2^{-/-} knockout mice (Rag2tm1Fwa)53 were also used in this study. Male and female mice were used in this study. RT7b rats were used for the generation of anti-PTBP3 monoclonal antibodies.

Policy information about [studies involving human research participants](#)

12. Description of human research participants

Describe the covariate-relevant population characteristics of the human research participants.

The study did not involve human research participants.

ChIP-seq Reporting Summary

Form fields will expand as needed. Please do not leave fields blank.

▶ Data deposition

1. For all ChIP-seq data:

- a. Confirm that both raw and final processed data have been deposited in a public database such as [GEO](#).
- b. Confirm that you have deposited or provided access to graph files (e.g. BED files) for the called peaks.

2. Provide all necessary reviewer access links.
The entry may remain private before publication.

The data has been deposited in GEO: GSE100969 accession number
The token efercweczvizhgd gives access to it, until it is made publicly available

3. Provide a list of all files available in the database submission.

The Fastq files for the five PTBP1 iCLIP replicates is available (GSM2698371 PTBP1 iCLIP replicate 1, GSM2698372 PTBP1 iCLIP replicate 2, GSM2698373 PTBP1 iCLIP replicate 3, GSM2698374 PTBP1 iCLIP replicate 4 and GSM2698375 PTBP1 iCLIP replicate 5)

In addition to the raw data, the following files are available:
GSE100969_PTBP1_B_LPS_All_peaks_id77424_lowFDR.bed.gz contains the processed significant PTBP1 binding sites from all the replicates together.
GSM2698371_PTBP1_B_LPS_1_peaks_id77154_lowFDR.bed.gz contains the processed significant PTBP1 binding sites from replicate 1.
GSM2698372_PTBP1_B_LPS_2_peaks_id77159_lowFDR.bed.gz contains the processed significant PTBP1 binding sites from replicate 2.
GSM2698373_PTBP1_B_LPS_3_peaks_id77150_lowFDR.bed.gz contains the processed significant PTBP1 binding sites from replicate 3.
GSM2698374_PTBP1_B_LPS_4_peaks_id77151_lowFDR.bed.gz contains the processed significant PTBP1 binding sites from replicate 4.
GSM2698375_PTBP1_B_LPS_5_peaks_id77155_lowFDR.bed.gz contains the processed significant PTBP1 binding sites from replicate 5.

4. If available, provide a link to an anonymized genome browser session (e.g. [UCSC](#)).

▶ Methodological details

5. Describe the experimental replicates.

5 biological replicates were carried out.

6. Describe the sequencing depth for each experiment.

iCLIP cDNA libraries were carried out with 20 to 27 PCR cycles. Random barcodes were used that allow unique reads identification. 267211, 300341, 62683, 532361 and 325568, unique reads mapping to the sense strand were obtained in the 5 biological replicates. 8192,8983,5354,13861 and 8963 unique reads mapping to the antisense strand were found in the 5 biological replicates.
Libraries were sequenced on a Illumina HiSeq 2000 platform on a 50 bp single-end mode.

7. Describe the antibodies used for the ChIP-seq experiments.

Anti-PTBP1 antibody (Thermofisher Catalog#: 32-4800), was used for iCLIP experiments. This antibody was validated by Western Blot (Supplementary

8. Describe the peak calling parameters. Figure 2a) and by flow cytometry (Supplementary Figure 2b).
9. Describe the methods used to ensure data quality. Peak calling was carried out as in König, J. et al. iCLIP reveals the function of hnRNP particles in splicing at individual nucleotide resolution. Nat. Struct. Mol. Biol. 17, 909–915 (2010).
Control experiments such as RNA digestion high RNase concentrations, immunoprecipitation without UV-light cross-linking and negative control isotype experiments were included.
10. Describe the software used to collect and analyze the ChIP-seq data. Analysis of the iCLIP and software used to process the raw reads are described in Online Methods

Flow Cytometry Reporting Summary

Form fields will expand as needed. Please do not leave fields blank.

▶ Data presentation

For all flow cytometry data, confirm that:

- 1. The axis labels state the marker and fluorochrome used (e.g. CD4-FITC).
- 2. The axis scales are clearly visible. Include numbers along axes only for bottom left plot of group (a 'group' is an analysis of identical markers).
- 3. All plots are contour plots with outliers or pseudocolor plots.
- 4. A numerical value for number of cells or percentage (with statistics) is provided.

▶ Methodological details

- | | |
|--|---|
| 5. Describe the sample preparation. | Single cell suspensions were prepared from tissues by passing the tissues through cell strainers with 70 and 40 μm pore sizes. |
| 6. Identify the instrument used for data collection. | BD LSRFortessa cytometers from BD Biosciences. |
| 7. Describe the software used to collect and analyze the flow cytometry data. | FlowJo versions 10.0.8r1 and 9.8.3. |
| 8. Describe the abundance of the relevant cell populations within post-sort fractions. | Purity of FACS-sorted samples was analysed by flow cytometry. Purity of the samples was >89%. |
| 9. Describe the gating strategy used. | Supplementary Figure 1e shows an exemplifying complete gating strategy of germinal centre B cells. Gates indicating boundaries between "positive" and "negative" are shown through out the figures with exemplifying plots. |

Tick this box to confirm that a figure exemplifying the gating strategy is provided in the Supplementary Information.